Naphthoquinone-induced arylation inhibits Sirtuin 7 activity

Valentina Sirri, Jérémy Berthelet, Oliver Brookes, Pascal Roussel

© 2022. Published by The Company of Biologists Ltd | Journal of Cell Science (2022) 135, jcs259207. doi:10.1242/jcs.259207

RESEARCH ARTICLE

Naphthoquinone-induced arylation inhibits Sirtuin 7 activity

Valentina Sirri, Jérémy Berthelet*, Oliver Brookes and Pascal Roussel‡

ABSTRACT

Natural or synthetic naphthoquinones have been identified to interfere with biological systems and, in particular, exhibit anticancer properties. As redox cyclers, they generate reactive oxygen species in cells and, as electrophiles, they react with nucleophiles, mainly thiols, and form covalent adducts. To further decipher the molecular mechanism of action of naphthoquinones in human cells, we analyzed their effects in HeLa cells. First, we demonstrated that the naphthoquinones menadione and plumbagin inhibited the nucleolar NAD^+-dependent deacetylase Sirtuin 7 *in vitro*. As assessed by their inhibition of rDNA transcription, pre-rRNA processing and formation of etoposide-induced 53BP1 foci, menadione and plumbagin also inhibited Sirtuin 7 catalytic activity *in vivo*. Second, we established that when sulfhydryl arylation by menadione or plumbagin was prevented by the thiol reducing agent N-acetyl-L-cysteine, the inhibition of Sirtuin 7 catalytic activity was also blocked. Finally, we discuss how inhibition of Sirtuin 7 might be crucial in defining menadione or plumbagin as anti-tumor agents that can be used in combination with other anti-tumor strategies.

KEY WORDS: rDNA transcription, pre-rRNA processing, 53BP1, Menadione, Plumbagin, SIRT7

INTRODUCTION

Quinones constitute a group of organic compounds that interact with biological systems. They can have inflammatory and anti-inflammatory effects (Checker et al., 2009), and exhibit properties that might be useful in cancer therapy (Qiu et al., 2018). The naphthoquinones are of particular interest as therapeutics as they occur naturally in a number of plants from which they are readily extracted. Naphthoquinones are also interesting from a toxicological perspective, because they are present in the atmosphere as bioactive environmental contaminants. In addition to passive exposure to naphthoquinones themselves, exposure to their precursor naphthalene, the major polynuclear aromatic hydrocarbon present in ambient air, is also significant. Naphthalene is biologically converted to naphthoquinones (Kumagai et al., 2012), and thus its inhalation also constitutes a potential route to naphthoquinone exposure.

Naphthoquinones act in cells through two main molecular mechanisms. First, as redox cyclers, they induce oxidative stress by generating reactive oxygen species (ROS) and second, as electrophiles, they react with nucleophiles, such as thiols or amines, and form adducts via the Michael addition reaction (Klotz et al., 2014). Several studies have shown that numerous cellular proteins go through covalent modification by electrophilic reactions with naphthoquinones and to a greater degree with quinones. For example, 2-methyl-1,4-naphthoquinone, also designated vitamin K_3 or menadione, was reported to inhibit *in vitro* protein tyrosine phosphatases (PTPs), most likely by arylating the cysteine residues present in their active sites, and to consequently activate the extracellular signal-regulated kinases 1 (ERK1, also known as MAPK3) and 2 (ERK2, also known as MAPK1) (Klotz et al., 2002). Consistent with this, 1,2-naphthoquinone was shown to negatively regulate the phosphatase PTP1B (also known as PTPN1) by forming covalent adducts and to cause a durable phosphorylation of epidermal growth factor receptor (Iwamoto et al., 2007). More recently, 1,4-benzoquinone and etoposide quinone, a reactive metabolite of etoposide, have been shown to alter PTPN2 catalytic activity by irreversibly forming a covalent adduct at the catalytic cysteine residue of the enzyme (Duval et al., 2019; Nian et al., 2019). Such an arylation reaction is also most likely responsible for the cdc25 inhibition induced by menadione (Wu and Sun, 1999) and by 2-(2-mercaptoethanol)-3-methyl-1,4-naphthoquinone, a synthetic thioalkyl vitamin K analogue called compound 5. Notably, the antiproliferative activity and phosphatase inhibition of compound 5 are antagonized by exogenous thiols but not by non-thiol antioxidants (Tamura et al., 2000).

The maintenance of cellular redox homeostasis involves different mechanisms, including the regulation by sirtuins (Singh et al., 2018). Indeed, mammalian sirtuins (Sirtuins 1–7, also known as SIRT1–SIRT7) are involved in the control of critical metabolic pathways such as stress response, apoptosis, DNA repair, cell cycle, genomic stability and gene expression. Sirtuins are protein deacetylases or ADP ribosyltransferases, also designated class III histone deacetylases (Blander and Guarente, 2004), and are composed of one conserved NAD-dependent catalytic core domain and of variable N-terminal and C-terminal extensions that contribute to their localization and substrate specificity. The most extensively studied sirtuin, Sirtuin 1, is mainly localized to the cell nucleus (Sun and Fang, 2016) and has many substrates including key redox-related transcription factors such as FOXO3a and p53 (Singh et al., 2018). Sirtuin 2 is a predominantly cytoplasmic protein during interphase (Michishita et al., 2005), and among the identified Sirtuin 2 deacetylation substrates, some are linked to redox homeostasis such as FOXO3a and NF-κB (Singh et al., 2018). The mitochondrial sirtuins (Sirtuins 3–5) (Michishita et al., 2005) have been reported to regulate the production of ROS in mitochondria, to be crucial in the repair of mitochondrial DNA and/or to be strongly associated with oxidative stress signaling (Singh et al., 2018). Nuclear Sirtuin 6 also participates in oxidative stress resistance (Wang et al., 2016) and was reported to be required for coactivation of the nuclear factor erythroid 2-related factor 2 (NRF2), one of the master regulators of antioxidant responses.

The last sirtuin, Sirtuin 7, is localized to nucleoli (Michishita et al., 2005), and was shown to be involved in rDNA transcription in

Université Paris Cité, Unité de Biologie Fonctionnelle et Adaptative (BFA), UMR 8251, CNRS, 4 rue Marie-Andrée Lagroua Weill-Hallé, F-75013 Paris, France. *Present address: Université Paris Cité, Centre Epigénétique et Destin Cellulaire (CEDC), UMR 7216, CNRS, 35 rue Hélène Brion, F-75013 Paris, France.

‡Author for correspondence (pascal.roussel@u-paris.fr)

V.S., 0000-0003-0961-8838; O.B., 0000-0003-0074-8644; P.R., 0000-0002-3093-669X

Handling Editor: Maria Carmo-Fonseca
Received 29 July 2021; Accepted 15 March 2022

Journal of Cell Science (2022) 135, jcs259207. doi:10.1242/jcs.259207

humans (Ford et al., 2006; Grob et al., 2009). It has been reported to be essential for early pre-rRNA processing (Chen et al., 2016), and especially for 45S pre-rRNA cleavage at site 2 (Sirri et al., 2019). Sirtuin 7 is directly implicated in DNA damage repair and in the maintenance of genome integrity (Tang et al., 2019; Vazquez et al., 2016). To date, there is no clear data regarding a possible role of Sirtuin 7 in the balance between the ROS production and antioxidant defenses. However, the fact that cellular stresses, which rapidly induce nucleolar oxidation, are often accompanied by dramatic changes in the organization and composition of nucleoli (Boulon et al., 2010), and that the morphology of nucleoli is intimately linked to nucleolar activities which are regulated by Sirtuin 7 (Sirri et al., 2019) raises the possibility that Sirtuin 7 might at least be sensitive to the redox status. Whatever the possible role of Sirtuin 7, nucleolar stress sensitivity involves a redox mechanism, as already established for the nucleoplasmic translocation of nucleolar protein nucleophosmin (NPM1, also called B23) (Yang et al., 2016).

To further decipher how naphthoquinones act in cells, we analyzed the effects of the naphthoquinones menadione, plumbagin and lawsone. First, we demonstrated that unlike lawsone, menadione and plumbagin inhibited the catalytic activity of Sirtuin 7 *in vitro*. As assessed by the inhibition of rDNA transcription, pre-rRNA processing and formation of etoposide-induced 53BP1 foci, menadione and plumbagin also inhibited the catalytic activity of Sirtuin 7 *in vivo*. Second, we established that in experimental conditions in which sulfhydryl arylation by menadione or plumbagin was prevented by the thiol reducing agent N-acetyl-L-cysteine (NAC), the menadione- or plumbagin-induced inhibition of Sirtuin 7 catalytic activity was also prevented. We discuss the importance of Sirtuin 7 in determining the efficacy of menadione or plumbagin as anti-tumor agents.

RESULTS

Naphthoquinones are highly cytotoxic. They induce oxygen free radicals and other reactive species (Klaus et al., 2010) which interact strongly with proteins and DNA. The introduction of carbonyl groups on certain amino acids can be used as a hallmark of the oxidation status of proteins, as seen in the metal-catalyzed oxidation of proteins (Stadtman, 1993). Similarly, DNA damage can be assessed by detecting the phosphorylation of the histone H2AX, which is involved in the formation of a stable repair complex at the site of DNA damage (Rogakou et al., 1998).

Some naphthoquinones induce oxidative modifications of proteins and DNA damage

To verify the effects of naphthoquinones on HeLa cells, cells were treated with naphthoquinones and compared with untreated cells or with cells treated with the DNA-damaging agent etoposide or the oxidizing agent tert-butyl hydroperoxide (tBHP). The oxidative modifications of proteins were then detected and quantified using the OxyBlot Protein Oxidation Detection Kit (Merck, Fig. 1Aa–c). For this purpose, cells were first lysed in the presence of 2% 2-mercaptoethanol to inhibit further oxidation, and the carbonyl groups in the protein side chains were derivatized to 2,4-dinitrophenylhydrazone (DNP-hydrazone). The mean values from three independent experiments showed that with the exception of lapachol and lawsone, the naphthoquinones rapidly induced an increase in the levels of derivatized carbonyl groups, which were higher than those observed for the positive control tBHP (Fig. 1Ac). As expected, this increase was not observed for cells treated with etoposide as a negative control.

To analyze the effects of naphthoquinones on DNA damage, HeLa cell extracts were prepared from untreated cells, cells treated with naphthoquinones and etoposide-treated cells. The cell extracts were then used to analyze histone H2AX phosphorylation (Fig. 1Ba). The mean values from three independent experiments showed that similar to the effects of etoposide, the naphthoquinones induced phosphorylation of the histone H2AX, with the exception of lapachol and lawsone, for which the signals obtained using the anti-phospho-H2AX antibody were comparable to those obtained in the absence of any treatment (Fig. 1Bb).

Menadione impairs DNA repair *in vivo* and Sirtuin 7 activity *in vitro*

To further analyze the effect of naphthoquinones on DNA repair, and more precisely on the recruitment of the DNA damage response factor 53BP1 (also known as TP53BP1) to DNA double-strand breaks, U2OS and HeLa cells were treated with etoposide or menadione, following which cells were immunolabeled using anti-phospho-H2AX and anti-53BP1 antibodies. We observed that untreated U2OS cells exhibited low levels of DNA damage (Fig. 2A) compared with untreated HeLa cells (Fig. S1). However, in agreement with the results obtained by immunoblotting (Fig. 1B), immunofluorescence labeling obtained with the anti-phospho-H2AX antibody largely increased after the etoposide and menadione treatments (Fig. 2Ae,h; Fig. S1e,h) compared to untreated cells (Fig. 2Ab; Fig. S1b). Unexpectedly, whereas the DNA-damaging agent etoposide induced the formation of 53BP1 foci (Fig. 2Af; Fig. S1f), menadione did not affect the localization of 53BP1 (compare Fig. 2Ac with Fig. 2Ai, and Fig. S1c with Fig. S1i) even if the phosphorylation of histone H2AX still occurred (Fig. 2Ah; Fig. S1h). The formation of 53BP1 foci was prevented by the presence of menadione but was still feasible, as observed after washing to remove menadione and culturing the cells for an additional 2 or 3 h (Fig. S2).

Because Sirtuin 7 was reported to regulate 53BP1 recruitment to damaged chromatin (Vazquez et al., 2016), we wondered if Sirtuin 7 activity was affected by tBHP or by naphthoquinones (namely, menadione, plumbagin and lawsone). For this purpose, we tested whether Sirtuin 7 could deacetylate the acetylated lysine 18 of histone H3 (H3K18-Ac) *in vitro* (Sirri et al., 2019). Purified recombinant Sirtuin 7 was preincubated with tBHP or naphthoquinones, and used to perform *in vitro* deacetylase assays on a fluorescent H3K18-Ac peptide. Deacetylation of the H3K18-Ac peptide was monitored and quantified as previously described (Duval et al., 2015) using reverse phase ultra-fast liquid chromatography (RP-UFLC). As observed in Fig. 2B, menadione and plumbagin significantly inhibited Sirtuin 7 deacetylase activity whereas lawsone did not. Interestingly, no significant effect on Sirtuin 7 activity was observed for the oxidizing agent tBHP.

Menadione and plumbagin impair rDNA transcription *in vivo*

Using siRNA-mediated Sirtuin 7 knockdowns, we and others have previously demonstrated that the activity of nucleolar Sirtuin 7 is essential for *in vivo* rDNA transcription (Ford et al., 2006; Grob et al., 2009). To build on this observation and to further clarify the effect of naphthoquinones on Sirtuin 7 *in vivo*, we analyzed the effects of menadione, plumbagin and lawsone on nucleolar 5-fluorouridine (FU) incorporation, i.e. on rDNA transcription. As shown in Fig. 3A, rDNA transcription was clearly visualized in untreated cells and in lawsone-treated cells, but little, if any, nucleolar FU incorporation was observed in menadione- or plumbagin-treated cells. To directly compare menadione-induced inhibition of Sirtuin 7 activity with that induced by sirtinol, a selective sirtuin inhibitor that effectively inhibits Sirtuin 7 catalytic

Journal of Cell Science (2022) 135, jcs259207. doi:10.1242/jcs.259207

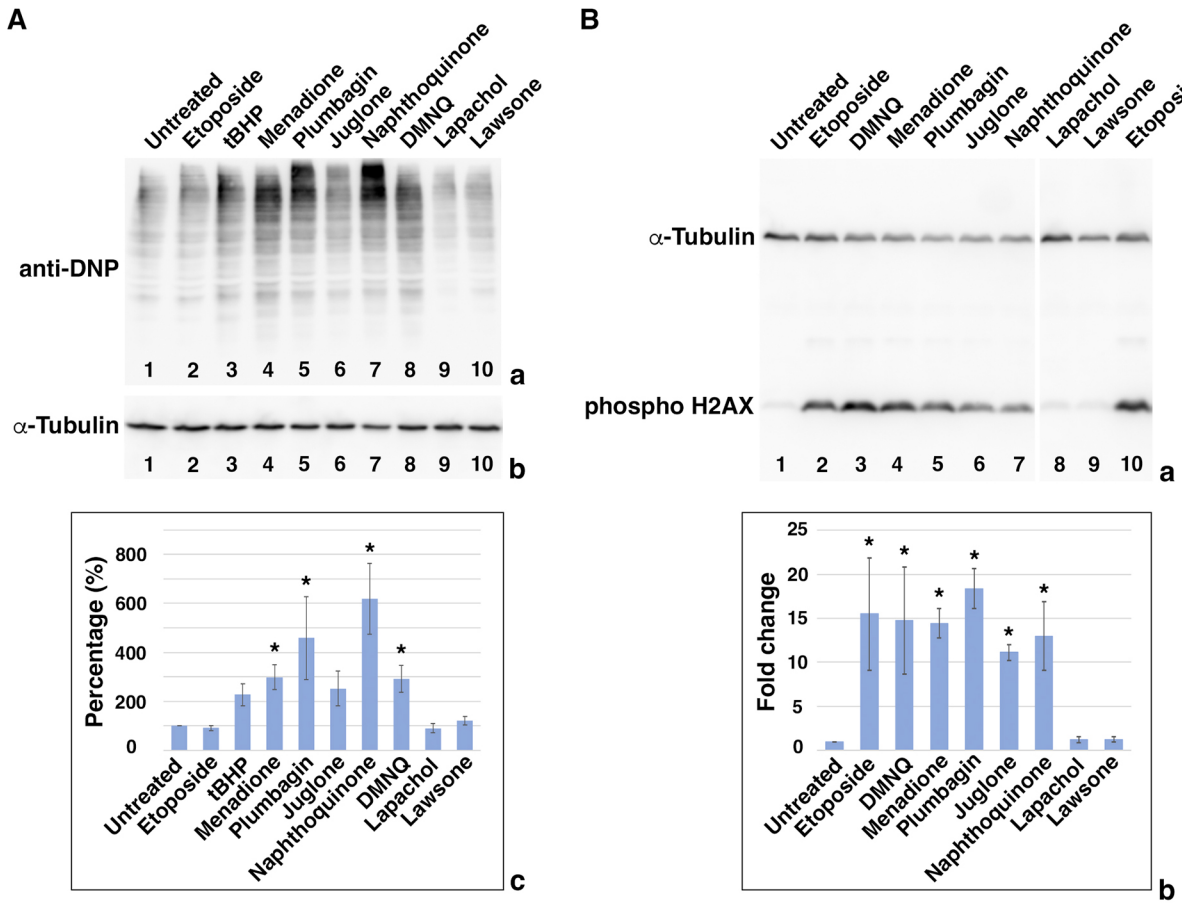

Fig. 1. Naphthoquinones induce oxidative modifications of proteins and DNA damage. (A) HeLa cells were treated with either etoposide (20 µM), tBHP (100 µM), menadione (40 µM), plumbagin (20 µM), juglone (20 µM), 1,4-naphthoquinone (20 µM), DMNQ (40 µM), lapachol (40 µM) or lawsone (40 µM) for 1 h. The oxidative modifications of proteins were detected and quantified using the OxyBlot Protein Oxidation Detection Kit. The DNP-derivatized proteins were separated by SDS-PAGE and revealed by immunoblotting using an anti-DNP antibody (a). After membrane stripping, immunoblotting was carried out using an anti-α-tubulin antibody (b). The anti-DNP signals were quantified for three independent experiments, including the one presented in Aa,b, normalized using the α-tubulin signals and averaged (c). The results are expressed as a percentage of the mean value for untreated cells. Error bars represent mean±s.d. **P*<0.05, one-way ANOVA followed by Dunnett's multiple comparison test. (B) HeLa cells were untreated or identically treated with etoposide or naphthoquinones. DNA damage was analyzed by detecting phospho-H2AX. Immunoblotting was simultaneously performed using anti-α-tubulin and anti-phospho-H2AX antibodies (a). The apparent white space in panel a corresponds to the limit of the two membranes used to constitute panel a. The anti-phospho-H2AX signals were quantified for three independent experiments including the one presented in Ba, normalized using the α-tubulin signals and averaged (b). The results are expressed as fold changes, i.e. ratios of the observed values to the mean value measured for untreated cells. Error bars represent mean±s.d. **P*<0.05, one-way ANOVA followed by Dunnett's multiple comparison test.

activity *in vitro* (Sirri et al., 2019), HeLa cells were treated with sirtinol or menadione. The nucleolar marker fibrillarin (FBL) was used to identify and delineate nucleoli (Fig. 3Ba) and to perform quantification of nucleolar FU incorporation, i.e. rDNA transcription, in an automated manner (Fig. 3Bb). The results showed that menadione inhibited rDNA transcription more efficiently than sirtinol.

Considering that menadione affects two Sirtuin 7-dependent functions, namely the formation of etoposide-induced 53BP1 foci and rDNA transcription *in vivo*, and also inhibits Sirtuin 7 activity *in vitro*, it seemed likely that menadione directly inhibits Sirtuin 7 activity. However, as it has been previously established that several quinones inhibit PTPs (Klotz et al., 2002; Iwamoto et al., 2007; Duval et al., 2019; Nian et al., 2019), we verified that menadione-induced impairment of DNA repair and inhibition of rDNA transcription described above was not caused by the inhibition of PTPs. We clearly observed that treatment with the PTP inhibitor sodium orthovanadate (Na_3VO_4) did not influence either etoposide-induced 53BP1 foci formation or rDNA transcription (Fig. S3), and therefore, the menadione-induced effects do not directly or indirectly result from the inhibition of PTPs.

Menadione and plumbagin impair pre-rRNA processing

To further elucidate the effects of menadione and plumbagin on nucleolar activity and to definitively establish that they inhibit *in vivo* Sirtuin 7 activity, we first investigated whether menadione treatment interfered with pre-rRNA processing, which, similarly to rDNA transcription, depends on the activity of Sirtuin 7. In particular, using siRNA-mediated Sirtuin 7 depletion, we previously established that Sirtuin 7 is primarily essential for 45S pre-rRNA cleavage at site 2 (Sirri et al., 2019). To more directly evaluate the effect of menadione on pre-rRNA maturation, rDNA transcription was suppressed by using actinomycin D (AMD), which has been shown to induce a total inhibition of rDNA transcription within 10 min (Popov et al., 2013). Total RNA was extracted from HeLa cells treated with AMD only or with AMD and menadione for increasing lengths of time, and from untreated cells. They were analyzed by northern blotting using the external

Journal of Cell Science (2022) 135, jcs259207. doi:10.1242/jcs.259207

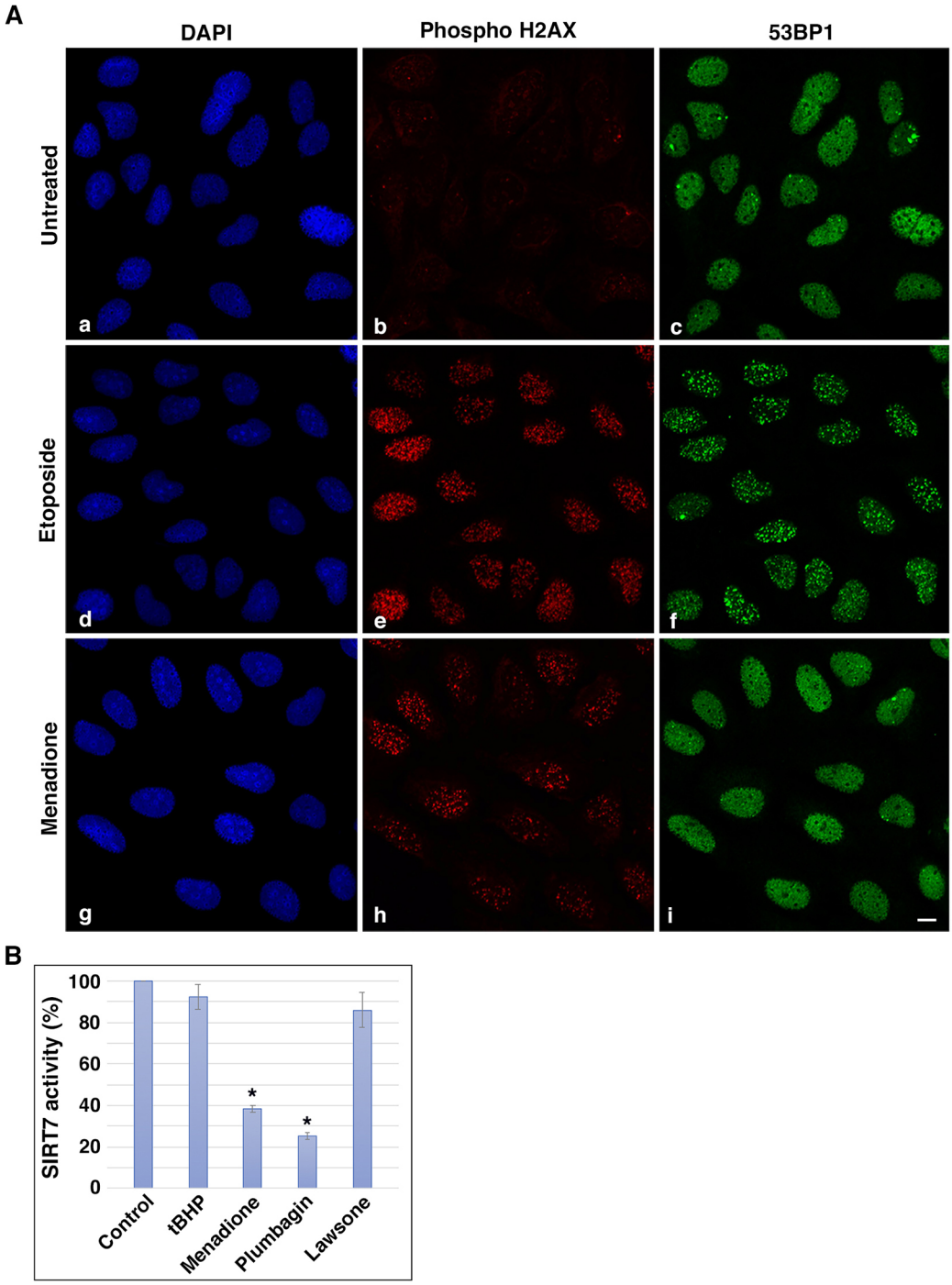

Fig. 2. Menadione impairs DNA repair *in vivo* and Sirtuin 7 activity *in vitro*. (A) The recruitment of 53BP1 to DNA double-strand breaks was analyzed in U2OS cells that were untreated (a–c), treated with etoposide (20 µM) (d–f) or menadione (60 µM) (g–i) for 30 min. Immunofluorescence labeling was performed using anti-phospho-H2AX (b,e,h) and anti-53BP1 (c,f,i) antibodies. z-maximum projections are shown. Images are representative of three independent experiments. Scale bar: 10 µm. (B) Purified recombinant human Sirtuin 7 was first preincubated with DMSO, tBHP (100 µM), menadione (40 µM), plumbagin (20 µM) or lawsone (40 µM) for 30 min at room temperature, and *in vitro* Sirtuin 7 deacetylase assays were performed on 50 µM fluorescent H3K18-Ac peptides in the presence of 6 mM NAD^+ for 2 h at 37°C. Results are expressed as a percentage of the control values (i.e. values obtained with preincubation of recombinant human Sirtuin 7 with DMSO). Error bars represent mean±s.d. n=3. *P<0.05, one-way ANOVA followed by Dunnett's multiple comparison test.

transcribed spacer (ETS) probe (Fig. 4A), allowing the detection of 47S, 45S and 30S pre-rRNAs. The levels of 47S/45S and 30S pre-rRNAs analyzed in the presence of menadione (Fig. 4A, lanes 2–5) were clearly higher than those seen in the absence of menadione (Fig. 4A, lanes 6–9). These results were similar to those obtained when similar experiments were performed using sirtinol (Sirri et al., 2019). This indicates that menadione treatment interferes with several pre-rRNA processing events, particularly with Sirtuin 7-dependent events such as 45S pre-rRNA cleavage at site 2 (Sirri et al., 2019), and therefore supports that menadione inhibits Sirtuin 7. This interference with pre-rRNA processing was also observed for plumbagin, but not for lawsone or tBHP, which do not exhibit

Journal of Cell Science (2022) 135, jcs259207. doi:10.1242/jcs.259207

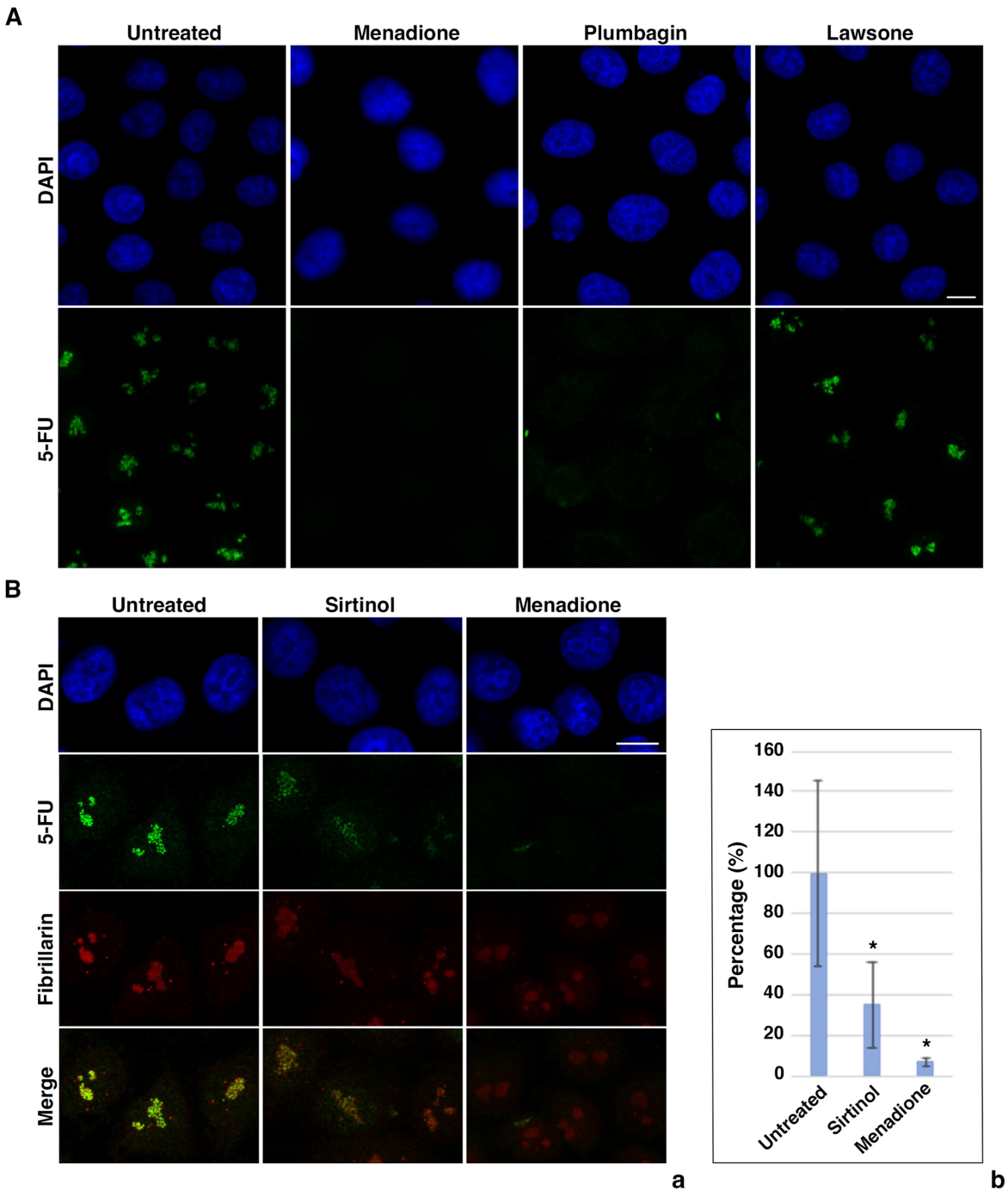

Fig. 3. Menadione and plumbagin impair rDNA transcription *in vivo*. (A) HeLa cells were treated with menadione (40 µM), plumbagin (4 µM) or lawsone (40 µM) for 1 h and cultured in medium containing 5-FU for the last 15 min of culture before being analyzed for 5-FU incorporation. Images are representative of three independent experiments. (B) HeLa cells were treated with sirtinol (100 µM) or menadione (40 µM) for 1 h, or not treated, and cultured in medium containing 5-FU for the last 15 min of culture before being processed to reveal 5-FU incorporation and fibrillarin. *z*-maximum projections of confocal immunofluorescence images representative of three independent experiments are shown (a). Scale bars: 10 µm. Quantification of rDNA transcription was conducted in an automated manner in at least 50 cells (b). The results were expressed as a percentage of the mean values of untreated cells. Error bars represent mean±s.d. **P*<0.05, Kruskal–Wallis test followed by Dunn's multiple comparison test.

any inhibitory effect on Sirtuin 7 activity *in vitro* (Fig. 2B), or for etoposide. As shown in Fig. 4B, northern blot analysis using the ETS probe showed that the 47S/45S and 30S pre-rRNAs were barely observed when the cells were treated with AMD alone or with AMD and etoposide, tBHP or lawsone. Conversely, they were clearly visible when the cells were treated with AMD and menadione or plumbagin, showing that pre-rRNA processing was notably slowed by these two naphthoquinones, suggesting that they exhibit inhibitory effects on Sirtuin 7 *in vitro* (Fig. 2B).

Menadione-induced inhibition of rDNA transcription and pre-rRNA processing is slowly reversed

As shown above, rDNA transcription and pre-rRNA processing, both Sirtuin 7-dependent functions, are impaired by menadione *in*

Journal of Cell Science (2022) 135, jcs259207. doi:10.1242/jcs.259207

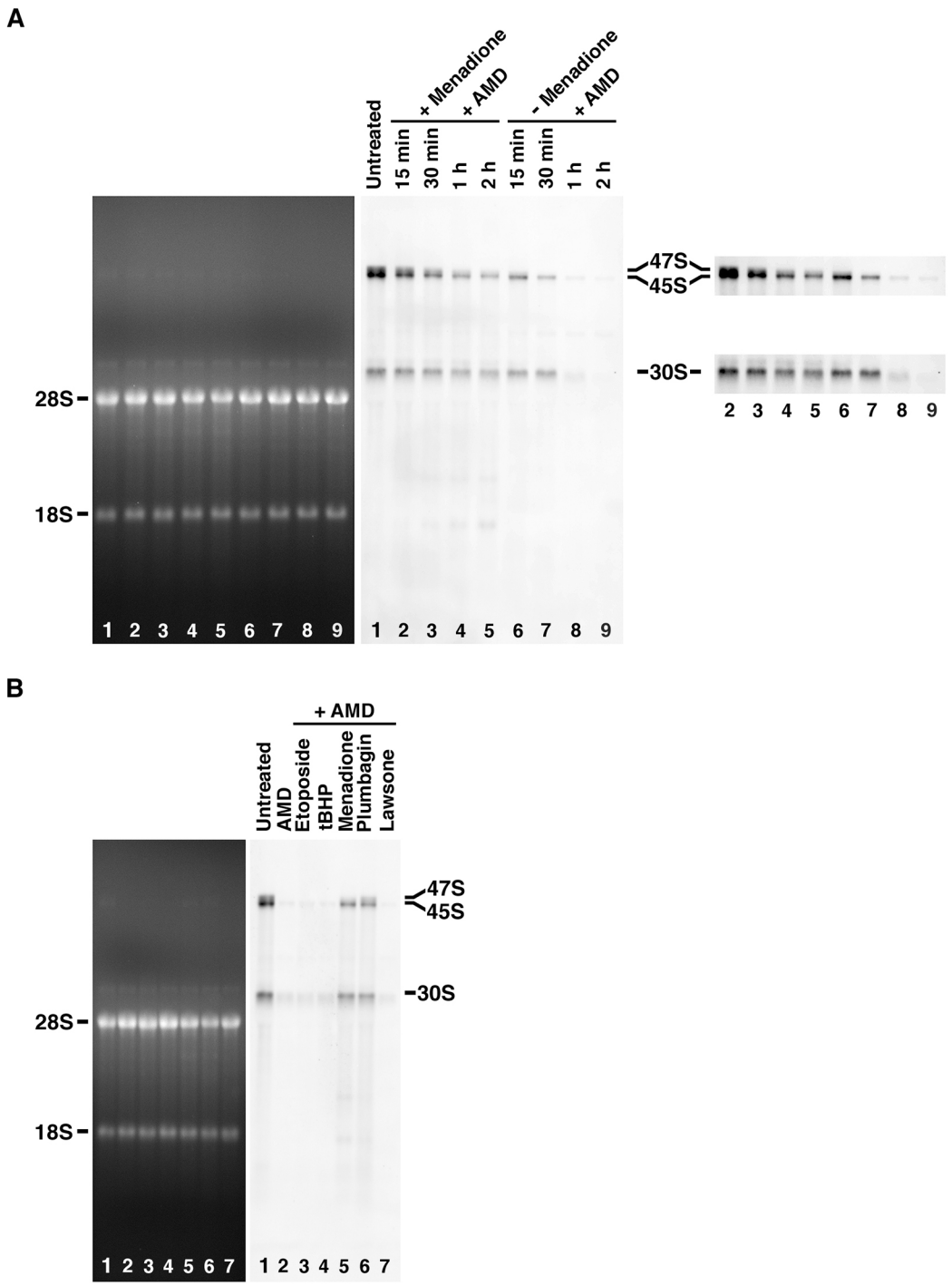

Fig. 4. Menadione and plumbagin impair pre-rRNA processing. (A) Total RNA was extracted from untreated HeLa cells and from HeLa cells treated for 15 min to 2 h with AMD or with AMD plus menadione (40 µM). Northern blot analysis was performed using the ETS probe allowing the detection of 47S, 45S and 30S pre-rRNAs. RNA loaded on the gel was detected by ethidium bromide staining (left) and northern blot analysis (middle), and cropped parts of the northern blot are presented on the right after applying a global intensity adjustment. (B) Total RNA was extracted from untreated HeLa cells and from HeLa cells treated for 1 h with AMD or with AMD plus either etoposide (20 µM), tBHP (100 µM), menadione (40 µM), plumbagin (20 µM) or lawsone (40 µM). RNA loaded on the gel was detected by ethidium bromide staining (left) and northern blot analysis performed using the ETS probe (right). Images are representative of three independent experiments.

vivo. To better assess menadione-mediated inhibition of Sirtuin 7 activity, we first wondered whether the effect of menadione on rDNA transcription was reversible. HeLa cells were treated with menadione for 30 min, and then, the cells were washed to remove menadione and cell culture was resumed for 30 min, 2 h or 3 h. In each condition, the cells were analyzed for FU incorporation and to localize fibrillarin used as a nucleolar marker. As shown in Fig. 5A, nucleolar rDNA transcription, indicated by FU incorporation, which was clearly visualized in untreated cells, was no longer observed in cells treated with menadione. However, the inhibition of rDNA transcription was apparently released after the removal of menadione, and therefore, FU incorporation was observed 2 or 3 h

Journal of Cell Science (2022) 135, jcs259207. doi:10.1242/jcs.259207

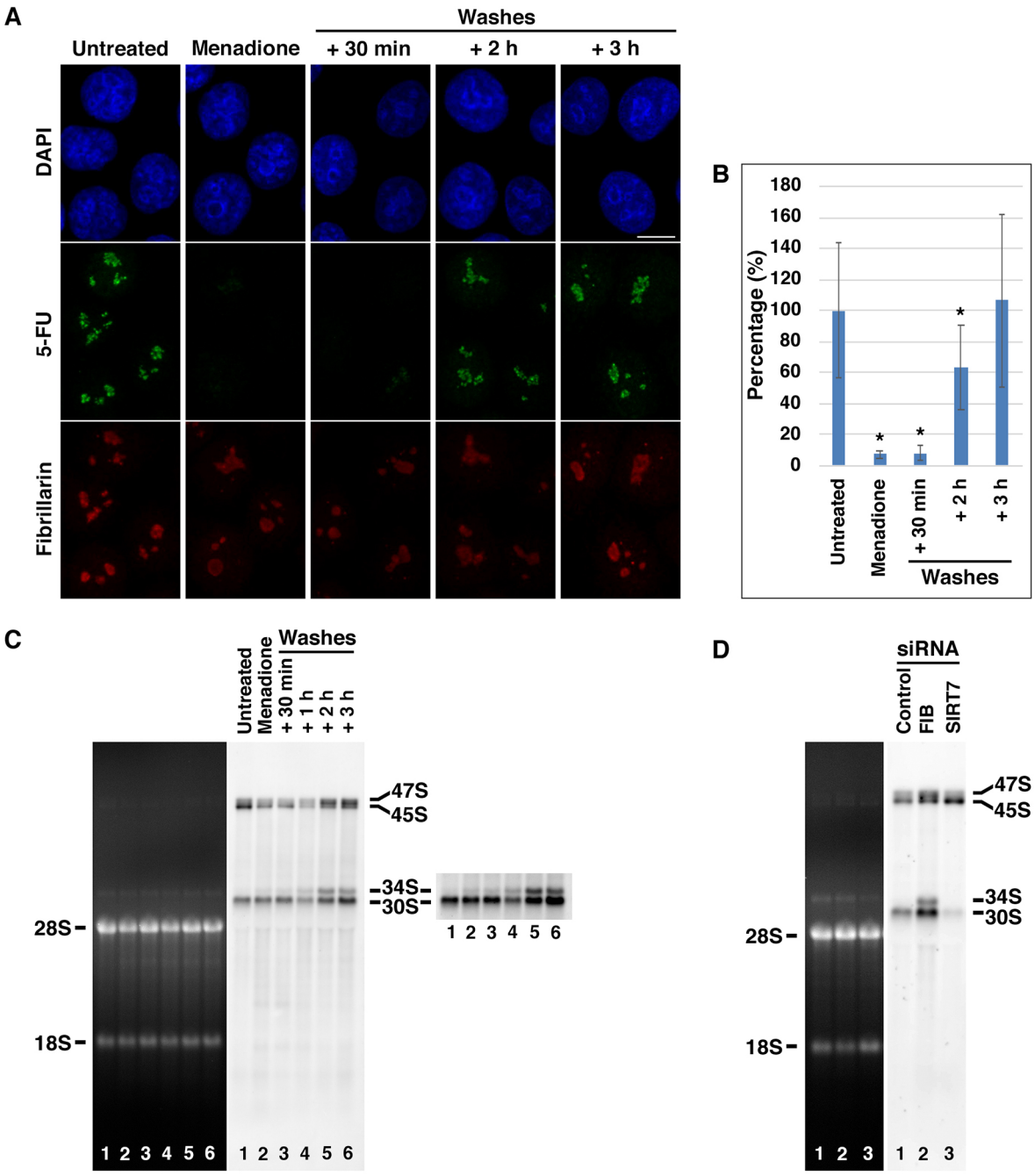

Fig. 5. Menadione-induced inhibition of rDNA transcription and pre-rRNA processing is slowly reversed. (A) HeLa cells were treated with menadione (40 µM) for 30 min and then washed and cultured further without menadione for 30 min, 2 h or 3 h. In all cases, cells were cultured in medium containing 1 mM 5-FU for the last 15 min of culture before being analyzed for 5-FU incorporation and the nucleolar marker fibrillarin. *z*-maximum projections are shown. Scale bar: 10 µm. (B) Quantification of rDNA transcription conducted in an automated manner in at least 50 cells. Results are expressed as a percentage of the mean values of untreated controls. Error bars represent mean±s.d. **P*<0.05, Kruskal–Wallis test followed by Dunn's multiple comparison test. (C) Total RNA was extracted from untreated HeLa cells, from HeLa cells treated with menadione (40 µM) for 30 min, and from HeLa cells treated with menadione (40 µM) for 30 min and then washed and cultured further without menadione for 30 min, 1 h, 2 h or 3 h. RNA was detected by ethidium bromide staining (left) and northern blot analysis performed using the ETS probe (middle), and the cropped part of the northern blot analysis is presented on the right after applying a global intensity adjustment. (D) Total RNA was extracted from HeLa cells transfected with control siRNAs, or with siRNAs targeting fibrillarin or Sirtuin 7. Northern blot analysis was then performed using the ETS probe. Images are representative of three independent experiments.

after washes (Fig. 5A). Automated quantification of rDNA transcription from at least 50 cells (Fig. 5B) confirmed that the *in vivo* menadione-mediated inhibition of rDNA transcription was gradually released after the removal of menadione, i.e. after washing and culture in a fresh menadione-free culture medium. As for pre-rRNA processing, total RNA was prepared from untreated HeLa cells, HeLa cells treated with menadione and menadione-treated HeLa cells that were washed and cultured without menadione for various durations, as described above. Northern blot analysis using the ETS probe showed that, in accordance with the observed inhibition of rDNA transcription by menadione, 47S/45S pre-rRNA levels decreased in cells treated with menadione (Fig. 5C, compare

Journal of Cell Science (2022) 135, jcs259207. doi:10.1242/jcs.259207

lanes 1 and 2) and this occurred in spite of the menadione-induced defect of pre-rRNA processing noted above (Fig. 4). Conversely, rDNA transcription and pre-rRNA processing resumed after washing the cells of menadione. The resumption of rDNA transcription can be inferred from the accumulation of 47S/45S and 30S pre–rRNAs, which were visible from 1 h after the removal of menadione (Fig. 5C, lanes 4–6). The increase of 45S and 30S pre-rRNAs also demonstrates that pre-rRNA processing occurred in cells after removal of menadione. The increase of 30S pre-rRNA implied the cleavage of the 45S pre-rRNA at site 2, which involves Sirtuin 7 activity (Sirri et al., 2019), as demonstrated by comparing pre-rRNA profiles in control cells and Sirtuin 7-depleted cells (Fig. 5D, compare lanes 1 and 3). Even if Sirtuin 7 activity was slowly restored, it was noteworthy that the pre-rRNA patterns obtained after 2 h (Fig. 5C, compare lanes 1 and 5) or 3 h (Fig. 5C, compare lanes 1 and 6) of recovery were different from those seen in untreated cells, and therefore menadione-induced changes in the kinetics of some pre-rRNA processing steps remained at least 3 h after removal of menadione. In particular, an accumulation of 47S, 34S and 30S pre-rRNAs and a decrease of 45S pre-rRNA, i.e. the lower band of the doublet visible in the upper part of the pre-rRNA patterns, were observed. All these changes could be explained by a defect in the cleavages of pre-rRNAs involving box C/D small nucleolar ribonucleoprotein particles (snoRNPs) such as the U3 snoRNP (Langhendries et al., 2016). This argument is supported by the fact that these results can be reproduced by siRNA-mediated depletion of fibrillarin, one of the four core proteins present in all box C/D snoRNPs (Fig. 5D, compare lanes 1 and 2). As better evidenced after applying a global intensity adjustment (Fig. 5C, lanes 1–6), 34S pre-rRNA was scarce in menadione-treated HeLa cells but became more abundant after removal of menadione, i.e. when rDNA transcription and slightly modified pre-rRNA processing were restored.

However, the fact that menadione-induced inhibition of rDNA transcription, pre-rRNA processing (Fig. 5) and formation of 53BP1 foci (Fig. S2) were reversed after about 3 h without menadione showed that Sirtuin 7 activity was slowly restored. It also raised the question of whether the resumption of Sirtuin 7 activity was actually due to the release of Sirtuin 7 inhibition or due to newly synthesized Sirtuin 7. To ascertain this, we analyzed the formation of 53BP1 foci in the presence of cycloheximide (CHX), a protein synthesis inhibitor. The recruitment of 53BP1 to DNA double-strand breaks was analyzed in U2OS cells that were treated with 60 µM menadione for 30 min, washed and cultured for an additional 3 h with or without CHX. Etoposide was added for the last 30 min of culture and the formation of 53BP1 foci was compared (Fig. S4A). We clearly observed that in the presence of CHX, the menadione-induced inhibition of 53BP1 foci formation was not reversed. In the absence of menadione treatment, CHX exposure did not inhibit the etoposide-induced formation of 53BP1 foci in U2OS cells (Fig. S4B), and thus, it is likely that the resumption of Sirtuin 7 activity was actually because of Sirtuin 7 synthesis and not due to the release of Sirtuin 7 inhibition. However, we cannot exclude that the resumption of Sirtuin 7 activity was linked to protein synthesis without being directly due to the synthesis of Sirtuin 7.

NAC counteracts menadione- or plumbagin-induced effects

Our results showed that certain naphthoquinones, in particular menadione and plumbagin, inhibited Sirtuin 7 both *in vitro* and *in vivo*, whereas others, such as lawsone or lapachol, had no effect. Consequently, we wondered what mechanism could explain the naphthoquinone-induced inhibition of Sirtuin 7. Because menadione and plumbagin induce oxidative modifications of proteins (Fig. 1A), we wondered whether naphthoquinone-induced Sirtuin 7 inhibition was caused by oxidative modifications even though the oxidizing agent tBHP had no significant effect on Sirtuin 7 activity. To test this hypothesis, we performed immunoprecipitation of Sirtuin 7 and analyzed its oxidative modifications. HeLa cells expressing Sirtuin 7 tagged with green fluorescent protein (GFP) were treated with menadione and then lysed in the presence of 1% 2-mercaptoethanol, thus inhibiting further oxidation. The lysates were then processed for GFP–Sirtuin 7 immunoprecipitation. Potential oxidative modifications of GFP–Sirtuin 7 were detected and quantified using the OxyBlot Protein Oxidation Detection Kit. DNP-derivatized protein samples were separated and revealed by immunoblotting using first the anti-DNP antibody and then the anti-Sirtuin 7 antibody (Fig. S5). Our results did not show any oxidative modification of the GFP–Sirtuin 7 immunoprecipitated from extracts prepared from menadione-treated cells for which, as expected, the global levels of oxidized proteins were increased. In accordance with the fact that tBHP had no significant effect on Sirtuin 7 activity, it was therefore very unlikely that inhibition of Sirtuin 7 is linked to oxidative modifications of the protein.

Menadione and plumbagin have redox-cycling activity but also thiol (sulfhydryl)-reactive properties, as evidenced by their UV–visible absorption spectra in the presence and absence of the thiol reducing agent N-acetyl-L-cysteine (NAC) (Vasudevarao et al., 2014). Indeed, NAC addition resulted in changes to the UV–visible absorption spectra of plumbagin (Fig. 6Ac) and menadione (Fig. 6Ad). Conversely, the UV–visible absorption spectra of lawsone, which is unable to react with NAC (Vasudevarao et al., 2014), and of the non-alkylating redox-cycling quinone 2,3-dimethoxy-1,4-naphthoquinone (DMNQ) were not influenced by NAC (Fig. 6Aa,b).

NAC also influences the menadione- or plumbagin-induced phosphorylation of ERK (here referring to ERK1/2) in HeLa (Fig. 6B,C). Menadione-induced ERK phosphorylation was found to be the consequence of PTP inhibition by sulfhydryl arylation and not by redox cycling (Klotz et al., 2002; Carr et al., 2002), and accordingly, ERK phosphorylation was observed in HeLa cells treated with menadione or plumbagin (Fig. 6B, compare lanes 1, 7 and 9), but not in HeLa cells treated with compounds inducing redox cycling such as hydrogen peroxide or DMNQ (Fig. 6B, compare lanes 1, 3 and 5). It is noteworthy that even if redox cycling was previously excluded as the main mechanism responsible for ERK phosphorylation following menadione treatment, Klotz et al. (2002) reported that DMNQ treatment induced ERK phosphorylation in WB-F344 rat liver epithelial cells. ERK phosphorylation was no longer observed in HeLa cells pre-treated with NAC prior to menadione or plumbagin treatment (Fig. 6B, compare lanes 2, 8 and 10; Fig. 6C), showing that NAC, by interfering with the thiol–reactive properties of menadione and plumbagin, completely abrogated the menadione- or plumbagin-induced effects in HeLa cells.

NAC counteracts menadione- or plumbagin-induced inhibition of rDNA transcription and pre-rRNA processing

Sirtuin 7 contains 11 cysteines, and, in particular, four cysteines (Cys195, Cys198, Cys225 and Cys228) in the Zn^{2+}-binding motif of the catalytic core (Mitra and Dey, 2020). Hence, we wondered whether sulfhydryl arylation could explain *in vivo* menadione- and plumbagin-induced Sirtuin 7 inhibition as assessed by the inhibition of both rDNA transcription and pre-rRNA processing. To analyze the influence of NAC on the inhibition of rDNA transcription, HeLa cells were cultured in the presence of NAC for 2 h and then treated

Journal of Cell Science (2022) 135, jcs259207. doi:10.1242/jcs.259207

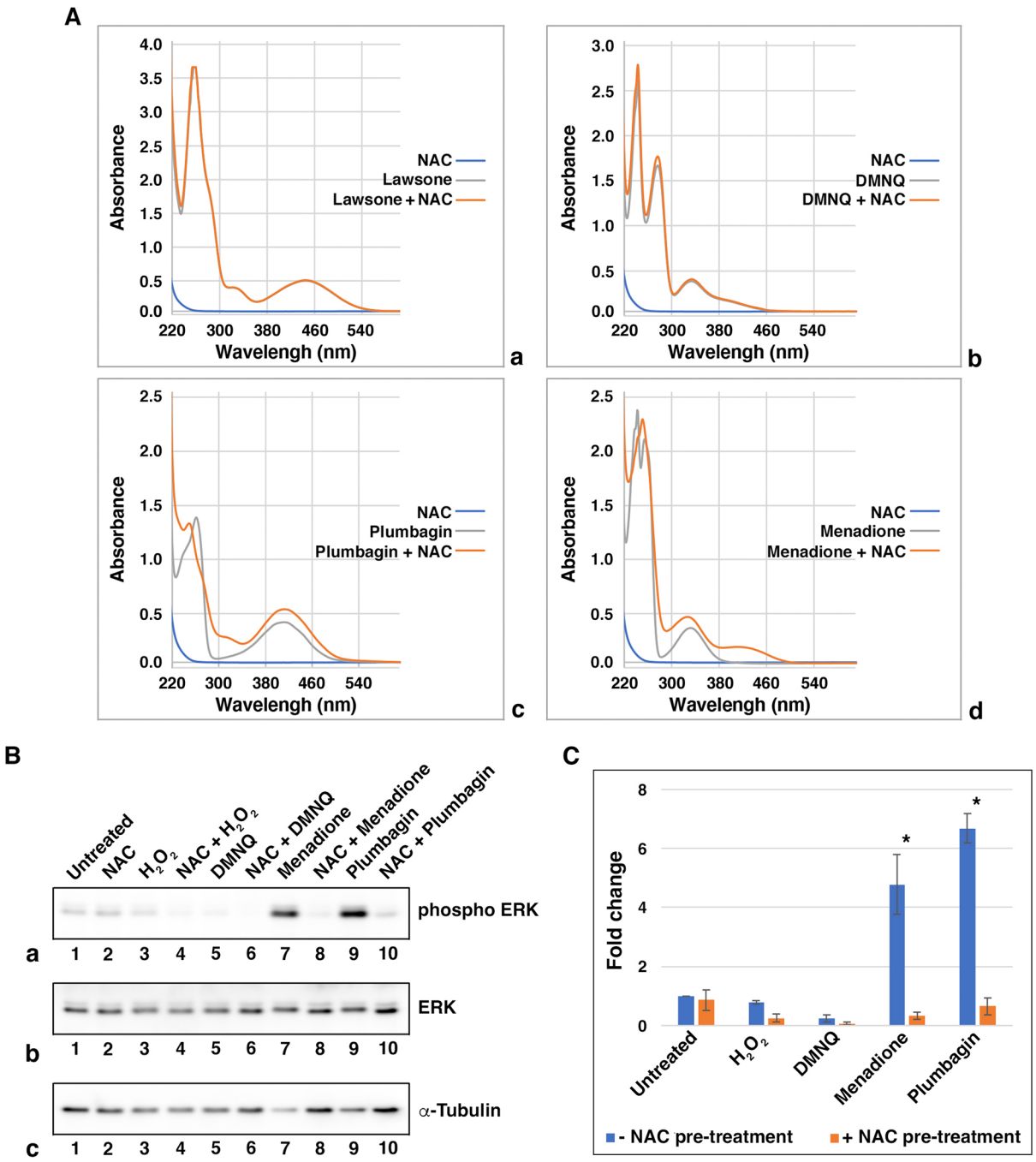

Fig. 6. NAC counteracts menadione- or plumbagin-induced effects. (A) UV–visible absorption spectra of lawsone (150 µM) and NAC (1.5 mM) alone and together (a), UV–visible absorption spectra of DMNQ (150 µM) and NAC (1.5 mM) alone and together (b), UV–visible absorption spectra of plumbagin (150 µM) and NAC (1.5 mM) alone and together (c) and those of menadione (150 µM) and NAC (1.5 mM) alone and together (d). (B) Protein extracts were prepared from HeLa cells that were pre-treated with NAC (10 mM) for 2 h and then treated with H_2O_2 (500 µM) for 20 min or with DMNQ (40 µM), menadione (40 µM) or plumbagin (20 µM) for 1 h, and then processed for immunoblotting with anti-phospho-ERK antibody (a). After membrane stripping, immunoblotting was carried out simultaneously using anti-ERK (b) and anti-α-tubulin (c) antibodies. (C) The anti-phospho-ERK signals were quantified for three independent experiments including the one presented in Ba, normalized using the ERK signals and averaged (mean±s.d.). The results are expressed as fold changes, i.e. ratios of the observed values to the mean value measured for untreated cells in the absence of NAC pre-treatment. Results without and with NAC pre-treatment were significantly different. *P<0.05, Mann–Whitney test.

with either menadione or plumbagin in the absence of NAC for 1 h. Nucleolar transcription activity, i.e. rDNA transcription, was assessed by FU metabolic labeling of RNAs synthesized during the last 15 min of culture, as done before (Fig. 3). Cells were analyzed for FU incorporation and the localization of the nucleolar marker fibrillarin (Fig. 7, 5-FU and Fibrillarin). Loss of FU incorporation after menadione and plumbagin treatment confirmed that both of them inhibited rDNA transcription efficiently, and fibrillarin labeling was decreased (Fig. 7, without pre-treatment). In addition, NAC reversed the menadione- or plumbagin-induced inhibition of rDNA transcription as well as the decrease in fibrillarin labeling (Fig. 7, NAC pre-treated cells).

Journal of Cell Science (2022) 135, jcs259207. doi:10.1242/jcs.259207

To address the influence of NAC on menadione- or plumbagin-induced impairment of pre-rRNA processing, total RNA was extracted from HeLa cells that were cultured in the absence or presence of NAC for 2 h, and then treated for 1 h with AMD or with AMD and menadione or plumbagin. RNA extracts were analyzed by northern blotting using the ETS probe (Fig. 8A), and 47S/45S or 30S pre-rRNA levels were measured for cells cultured with or without NAC, and treated with AMD alone, AMD and menadione, or AMD and plumbagin (Fig. 8B). The northern blot analyses confirmed that menadione and plumbagin slowed 47S/45S or 30S pre-rRNA processing (Fig. 8A, compare lanes 1, 3 and 5; Fig. 8B), and showed that NAC pre-treatment partially attenuated the impairment of pre-rRNA processing induced by menadione or plumbagin, with a stronger effect on plumbagin-treated cells. Nevertheless, it should be noted that the influence of NAC on rDNA transcription was measured during the last 15 min of treatment, whereas for pre-rRNA processing, the measurements reflect the entire duration of the treatments. Therefore, the latter measurements could be influenced more strongly by the difference in reactivity between NAC and the naphthoquinones and between the naphthoquinones and Sirtuin 7 cysteines. This could also explain why NAC appeared to counteract the effects of plumbagin more easily than those of menadione. In

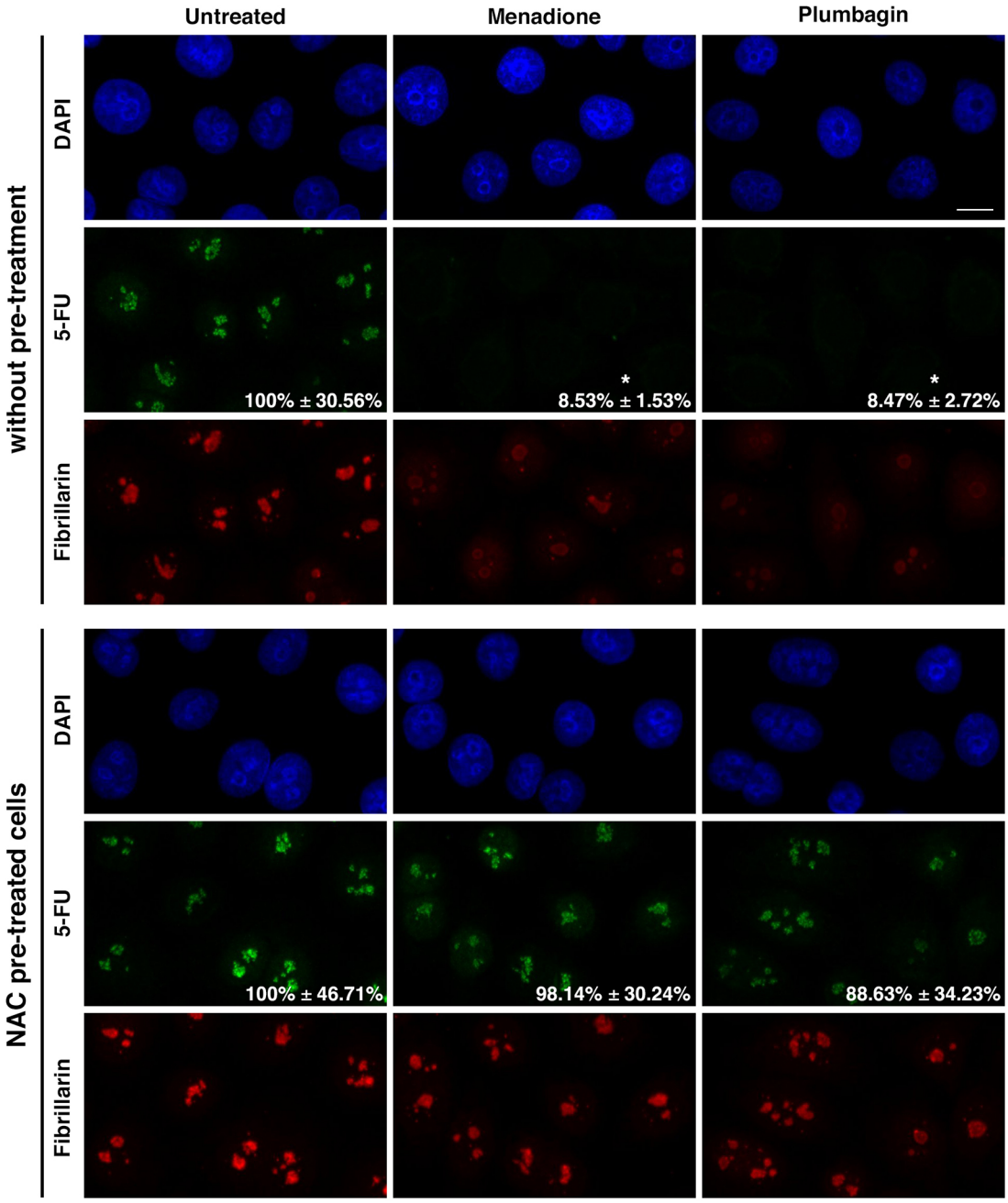

Fig. 7. NAC counteracts menadione- or plumbagin-induced inhibition of rDNA transcription. HeLa cells were cultured with or without NAC (10 mM) for 2 h and then treated with either menadione (40 µM) or plumbagin (20 µM) for 1 h. They were then cultured in a medium containing 5-FU for 15 min before being processed to reveal 5-FU incorporation and to observe fibrillarin. *z*-maximum projections representative of three independent experiments are shown. Scale bar: 10 µm. Numbers correspond to the quantification of rDNA transcription conducted in an automated manner in at least 50 cells and expressed as a percentage of the mean values of untreated cells (mean±s.d.). **P*<0.05, Kruskal–Wallis test followed by Dunn's multiple comparison test.

Journal of Cell Science (2022) 135, jcs259207. doi:10.1242/jcs.259207

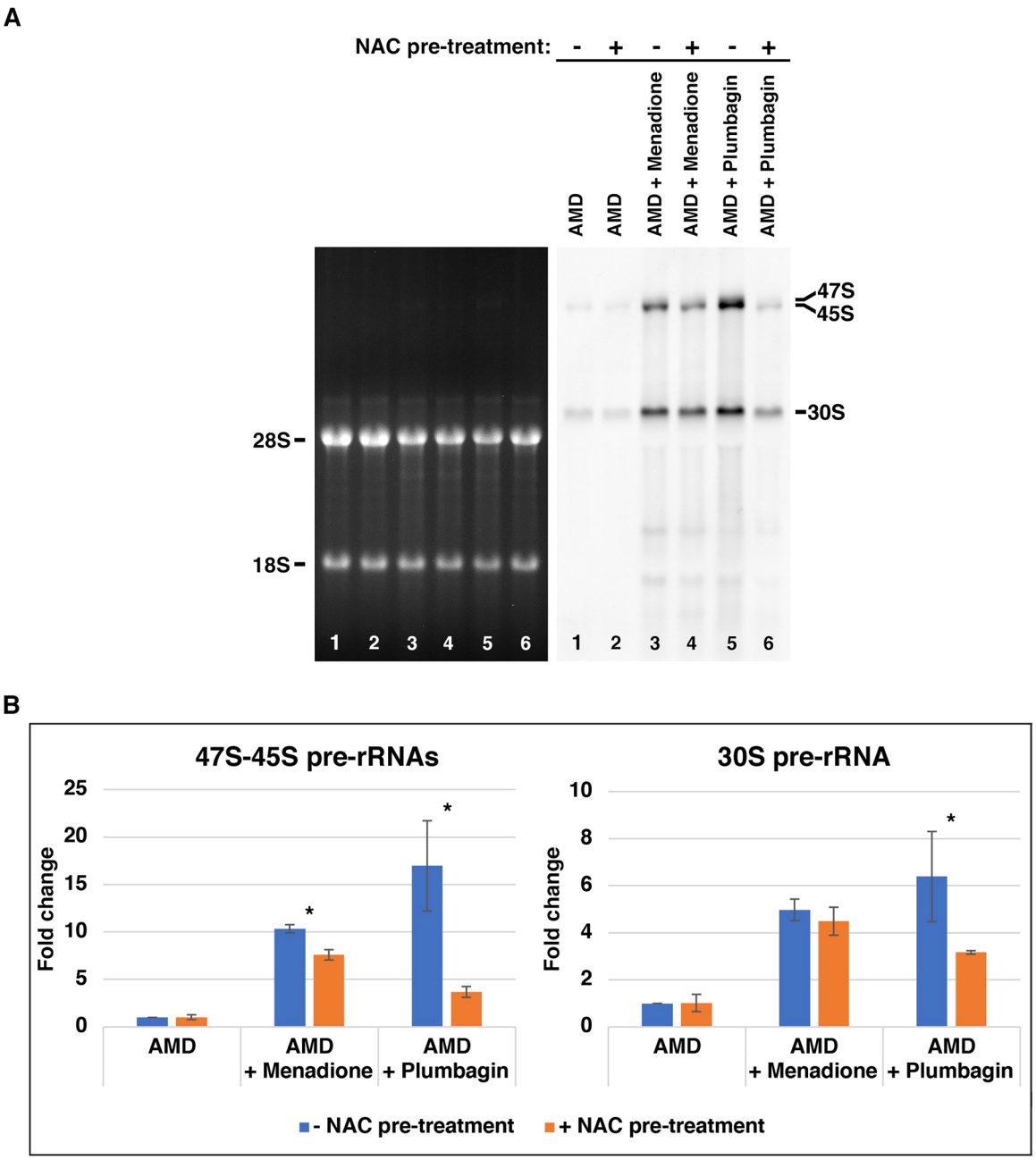

Fig. 8. NAC counteracts menadione- or plumbagin-induced inhibition of pre-rRNA processing. (A) Total RNA was extracted from HeLa cells cultured in the presence or absence of NAC (10 mM) for 2 h and then treated for 1 h with AMD alone or with AMD plus either menadione (40 µM) or plumbagin (20 µM). RNA extracts were analyzed by northern blots using the ETS probe. (B) Three independent experiments were quantified. The levels of 47S/45S and 30S pre-rRNAs were expressed as fold changes (mean±s.d.), i.e. ratios between the level of 47S/45S or 30S pre-rRNAs and that measured for cells cultured in the absence of NAC pre-treatment and treated with AMD alone. Results without and with NAC pre-treatment were significantly different. *P<0.05, Mann–Whitney test.

addition, because the processing of 47S/45S pre-rRNAs generates the 30S pre-rRNA (Sirri et al., 2019), the NAC pre-treatment-induced effects observed for the 47S/45S pre-rRNAs were more obvious than those observed for the 30S pre-rRNA (Fig. 8B).

Our results established that NAC attenuates menadione- or plumbagin-induced inhibition of rDNA transcription as well as menadione- or plumbagin-induced impairment of pre-rRNA processing. Consequently, it is most likely that NAC quenches naphthoquinone-mediated inhibition of Sirtuin 7 by preventing the menadione or plumbagin thiol-reactive property, i.e. the sulfhydryl arylation of Sirtuin 7 by menadione or plumbagin.

DISCUSSION

Quinones are widely distributed in nature and occur in animals and plants. They can be naturally present in the air or correspond to the metabolic products of molecules that can be inhaled. They often exhibit biological activities and therefore, they have been the subject of intensive research. Some of these compounds, especially 1,4-naphthoquinones, display anticancer activity, and thus, knowledge of their cellular targets is essential to understand their molecular mechanisms of action as anti-tumor agents.

A general mechanism to be considered first is that quinones participate in the cell redox cycle and act as precursors of ROS

Journal of Cell Science (2022) 135, jcs259207. doi:10.1242/jcs.259207

which possibly leads to severe oxidative stress, and consequently, to oxidation of cellular macromolecules such as DNA, RNA, lipids and proteins (Klotz et al., 2014; Wellington, 2015). The increase of intracellular ROS concentration mostly affects proteins by leading to the accumulation of carbonyl and thiol groups, and therefore, affects protein structure and function.

Beyond this general mechanism, naphthoquinones previously recognized as potent cell growth inhibitors, such as menadione, compound 5 and PD 49, have been shown to be selective inhibitors of Cdc25 phosphatases (Kar et al., 2003; Tamura et al., 2000; Wu and Sun, 1999) that regulate different aspects of cell cycle progression. Interestingly, plumbagin exhibits anticancer activity because of its inhibition of cell proliferation, induction of apoptosis, and its anti-invasive and anti-angiogenic properties (Tripathi et al., 2019). Plumbagin might act as a signaling modulator in cancer. Indeed, in human gastric cancer cells, plumbagin potentiates apoptosis by inhibiting the NF-κB signaling pathway (Jing et al., 2012). Moreover, in esophageal cancer cells, plumbagin abrogates the signal transducer and activator of transcription 3 (STAT3)-Polo-like kinase 1 (PLK1)-protein kinase B (AKT) signaling pathway (Cao et al., 2018). Plumbagin suppresses STAT3 activation through inducing SH2-containing protein tyrosine phosphatase 1 (SHP1) as shown in human multiple myeloma cells (Sandur et al., 2010) and human gastric cancer cells (Joo et al., 2015). In contrast, quinones have been shown to positively regulate STAT signaling in human hematopoietic cells. Indeed, 1,4-benzoquinone and etoposide-quinone were found to lead to the inhibition of endogenous PTPs (Duval et al., 2019; Nian et al., 2019), and consequently increased STAT1 phosphorylation and the expression of STAT1-regulated genes upon stimulation with interferon γ (IFNγ).

Here we established that naphthoquinones, namely menadione and plumbagin, impair Sirtuin 7 activity *in vitro*. Menadione interferes with DNA repair *in vivo*, in particular by preventing Sirtuin 7-dependent recruitment of 53BP1 to DNA double-strand breaks. Similarly, menadione and plumbagin alter rDNA transcription and pre-rRNA processing *in vivo*, functions which both require Sirtuin 7 activity (Sirri et al., 2019). Although menadione and plumbagin directly impair Sirtuin 7 activity *in vitro*, we verified that the effects observed *in vivo* do not result from the inhibition of PTPs. Indeed, formation of etoposide-induced 53BP1 foci and rDNA transcription are not influenced by treatment with the PTP inhibitor Na_3VO_4. Consequently, we concluded that menadione and plumbagin quickly and efficiently inhibit Sirtuin 7 activity *in vitro* and *in vivo*. The menadione or plumbagin-induced effects were not reproduced by the oxidizing agent tBHP and the inhibition of Sirtuin 7 appeared not to be related to oxidative modifications. Thus, the mechanism of inhibition is likely not the result of the redox cycling activity and more likely because menadione or plumbagin might react as electrophiles with nucleophiles, such as thiols, and form adducts (Klotz et al., 2014). Similar arylation reactions have previously been shown to alter the catalytic activity of PTPN2 (Duval et al., 2019; Nian et al., 2019) by irreversibly forming a covalent adduct at the catalytic cysteine residues of the enzymes. In this study, we found that menadione-induced inhibition of rDNA transcription, pre-rRNA processing and formation of etoposide-induced 53BP1 foci was slowly reversed after about 3 h without menadione. However, this observation does not dispute the irreversibility of Sirtuin 7 inhibition. Indeed, as shown for the formation of etoposide-induced 53BP1 foci, the recovery takes place only under experimental conditions in which protein synthesis is possible, i.e. in the absence of CHX. Thus, the resumption of Sirtuin 7 activity likely depends on newly synthesized proteins and is not due to the release of Sirtuin 7 inhibition. If an arylation reaction were to occur, Sirtuin 7 contains 11 cysteines in its sequence and, in particular, four cysteines (Cys195, Cys198, Cys225 and Cys228) in the Zn^{2+}-binding motif of the catalytic core (Mitra and Dey, 2020). Furthermore, unlike lawsone which does not impair Sirtuin 7 activity *in vivo*, menadione and plumbagin share a thiol-reactive property, as evidenced by changes in their UV–visible absorption spectra in the presence of the thiol-reducing agent NAC (Vasudevarao et al., 2014; this study). More interestingly, when the menadione- or plumbagin-induced inhibition of PTPs by sulfhydryl arylation, as assessed by the phosphorylation of ERK (Klotz et al., 2002; Carr et al., 2002; this study) was prevented by NAC, the menadione- or plumbagin-induced inhibition of rDNA transcription and pre-rRNA processing was also prevented. Thus, menadione- or plumbagin-induced Sirtuin 7 inhibition therefore clearly depends on arylation reactions.

Regardless of how menadione- and plumbagin-induced Sirtuin 7 inhibition occurs, it affects rDNA transcription and pre-rRNA processing. More generally, Sirtuin 7 inhibition affects ribosome biosynthesis and therefore counteracts the increased need for protein synthesis in cancer cells. In addition, menadione and plumbagin could inhibit rDNA transcription and thus disrupt nucleoli and activate p53-dependent apoptotic signaling, resembling the effects of the small molecule CX–5461, a selective inhibitor of RNA Polymerase I (Bywater et al., 2012). Indeed, rDNA transcription can be therapeutically targeted with CX-5461 to selectively kill B-lymphoma cells *in vivo* while viably maintaining a wild-type B cell population. A Sirtuin 7 inhibitor (ID: 97491) has been reported to affect cell proliferation and apoptosis in human uterine sarcoma cells and inhibits cancer growth *in vivo* (Kim et al., 2019). Furthermore, Sirtuin 7 activity is essential for DNA damage repair at several levels, not only for the recruitment of 53BP1 to DNA double-strand breaks (Vazquez et al., 2016; this study), but also for the deacetylation of the ataxia-telangiectasia mutated (ATM) kinase, and thus its regulation, and consequently for regulation of the DNA damage checkpoint (Tang et al., 2019).

In addition to inhibiting cell proliferation, migration and tumor growth *in vivo*, Sirtuin 7 depletion also increases drug sensitivity by activating the p38MAPK signaling pathway in breast cancer cells (Chen et al., 2018) and induces radiosensitivity, which in turn triggers cell death in colorectal cancer cells and increases the effectiveness of chemoradiotherapy (Tang et al., 2017), suggesting that menadione or plumbagin could be used in combination with existing therapies in anticancer strategies.

Sirtuin 7 is one of the 7 human sirtuins, which are all composed of a conserved NAD-dependent catalytic domain and variable N- and C-terminal extensions (Blander and Guarente, 2004; Rajendran et al., 2011). Assuming that menadione- or plumbagin-induced inhibition of Sirtuin 7 is dependent on arylation reactions, and specifically on the arylation of catalytic cysteine residues, it could be hypothesized that because of the conserved NAD-dependent catalytic domain, the inhibition observed for Sirtuin 7 can be generalized to all sirtuins.

Although further studies are still needed to fully identify the targets of menadione and plumbagin in cells, particularly in cancer cells, inhibition of Sirtuin 7 is most likely critical in defining menadione or plumbagin as anti-tumor agents.

MATERIALS AND METHODS

Cell culture and treatments

HeLa cells, HeLa cells expressing GFP–Sirtuin 7 (Grob et al., 2009) and U2OS cells, recently authenticated and tested for contamination, were cultured in Roswell Park Memorial Institute (RPMI) medium with glutaMAX (GIBCO BRL) supplemented with 10% fetal calf serum (FCS,

GIBCO BRL) in a 5% CO_2 incubator at 37°C. AMD was used at 0.1 µg/ml for 15 min to 2 h, menadione at 40 µM for 15 min to 2 h on HeLa cells and at 60 µM for 30 min on U2OS cells, plumbagin at 4 µM to 20 µM for 1 h, lawsone at 40 µM for 1 h, lapachol at 40 µM for 1 h, juglone at 20 µM for 1 h, 1,4-naphthoquinone at 20 µM for 1 h, DMNQ at 40 µM for 1 h, tBHP at 100 µM for 1 h, H_2O_2 at 500 µM for 20 min, NAC at 10 mM for 2 h, Na_3VO_4 at 1 mM for 1 h or 4 h and CHX at 50 µg/ml for 3 h (all from Sigma-Aldrich). Sirtinol (Selleck) was used at 100 µM for 1 h and etoposide (TRC-Canada) at 20 µM for 30 min to 1 h.

Antibodies

The human autoimmune sera with specificity against fibrillarin (O61; 1:3000) was prepared as previously described (Sirri et al., 2002). The phospho-Tyrosine antibody (P-Tyr-100; 1:5000) was from Cell Signaling Technology. The anti-α-tubulin (clone DM1A; 1:1000) and anti-BrdU (clone BU-33; 1:500) antibodies were from Sigma-Aldrich. The anti-SIRT7 (C-3; 1:10,000), anti-β-Actin (AC-15; 1:10,000), anti-ERK 1/2 (C-9; 1:2000) and anti-phospho-ERK (E-4; 1:2000) antibodies were from Santa Cruz Biotechnology. The anti-53BP1 (PA5-54565; 1:3000) and anti-phospho-Histone H2AX (Ser139) (CR55T33; 1:3000) antibodies were from Thermo Fisher Scientific. The alkaline phosphatase-conjugated anti-digoxigenin (11 093 274 910; 1:20,000) antibody was from Roche. Secondary antibodies coupled to Alexa Fluor 488 (711-545-152 and 115-545-166; 1:500), Alexa Fluor 594 (711-585-150 and 109-585-088; 1:500) and horseradish peroxidase (115-035-003; 1:3000) were from Jackson ImmunoResearch Laboratories, Inc.

Probe

The ETS probe (Sirri et al., 2016) corresponding to human rDNA (nt +935/+1082) was generated by PCR as a digoxigenin-labeled oligonucleotide using human rDNA as a template, primers (ETS5, 5′-GTCGG-TGTGGGGTTCGAGGC-3′; ETS6, 5′-CCACCGCGATCGCTCACACG-3′) and the PCR DIG probe synthesis kit (Roche).

siRNA-mediated mRNA knockdown

The siControl RISC-free siRNA (Control siRNA) was from Dharmacon. The siRNAs targeting Sirtuin 7 (SIRT7 siRNA, 5′-GCCUGAAGGUU-CUAAAGATT-3′) and fibrillarin (FIB siRNA, 5′-GUCUUCAUUUGUC-GAGGAATT-3′) previously used (Sirri et al., 2019) were from Eurogentec. The siRNAs were transfected at 10 nM using INTERFERin™ (Polyplus-transfection) according to the manufacturer's instructions. All siRNAs were transfected 24 h and 48 h after cell seeding. Samples were prepared 24 h after the last transfection, and were analyzed by northern blotting.

Immunofluorescence labeling

To evaluate the level of rDNA transcription, cells were cultured in media containing 1 mM FU (Sigma-Aldrich) for the last 15 min of culture. The cells were fixed with methanol for 20 min at −20°C, air-dried for 5 min and rehydrated with PBS for 5 min. FU incorporation was then detected using anti-BrdU antibody labeled with Alexa-Fluor-488-conjugated anti-mouse antibody. Fibrillarin was detected simultaneously using the O61 serum labeled with Alexa-Fluor-594-conjugated anti-human antibody. 53BP1 was detected using the anti-53BP1 antibody labeled with Alexa-Fluor-488- or Alexa-Fluor-594-conjugated anti-rabbit antibodies, together with histone H2AX phosphorylated on serine 139, detected using the mouse monoclonal antibody labeled with Alexa-Fluor-594- or Alexa-Fluor-488-conjugated anti-mouse antibody. All preparations were mounted with the Fluoroshield antifading solution containing 4,6-diamidino-2-phenylindole (DAPI, Sigma-Aldrich). The cells were imaged by fluorescence microscopy performed using a Leica upright SP5 confocal microscope with a 40× objective and version 2.7.3 of the Leica Application Suite Advanced Fluorescence software. Multiple fluorophores were recorded sequentially at each *z*-step. Quantification was performed using ImageJ software (NIH).

Immunoblotting

Protein extracts were resuspended in SDS loading buffer (Laemmli, 1970) and boiled for 5 min at 100°C. These extracts or DNP-derivatized protein samples were resolved by 10% SDS-PAGE and transferred to nitrocellulose membranes (Protran, Schleicher & Schuell). For immunoblotting, the membranes were incubated first with primary antibodies and then with suitable horseradish peroxidase-conjugated secondary antibodies. The immunoreactivity was detected by chemiluminescence (GE Healthcare). If the membrane was to be analyzed with two antibodies, the membrane was either co-incubated with both antibodies or probed with the first antibody, stripped and re-probed with the second antibody. For this purpose, the membrane was incubated at 50°C for 5 min with some agitation in a pre-warmed stripping solution [100 mM 2-mercaptoethanol, 2% (w/v) SDS, 62.5 mM Tris-HCl, pH 6.8], rinsed under running tap water for 1 h and finally at 4°C overnight in TBS pH 7.5 (Euromedex) with 0.1% Tween-20 (Sigma-Aldrich). Immunoblotting was then performed using another primary antibody, followed by the suitable horseradish peroxidase-conjugated secondary antibody.

In vitro Sirtuin 7 deacetylase assay

In vitro Sirtuin 7 deacetylase assays were conducted based on the capacity of Sirtuin 7 to deacetylate H3K18-Ac (Barber et al., 2012). The fluorescent H3K18-Ac and H3K18 peptides used (Proteogenix, France) were previously reported (Duval et al., 2015). H3K18 peptide was used as a deacetylation control. Assays were performed in a total volume of 50 µl of deacetylase buffer (Tris 50 mM, pH 8, 150 mM NaCl) with 0.1 µg full-length recombinant human Sirtuin 7 (SRP5274, Sigma-Aldrich), 6 mM NAD^+, 50 µM H3K18-Ac peptide, 0.6 µg yeast tRNA (Sigma-Aldrich) and 1 mM dithiothreitol (DTT). Sirtuin 7 was first preincubated with vehicle (DMSO), tBHP (100 µM), menadione (40 µM), plumbagin (20 µM) or lawsone (40 µM) for 30 min at room temperature. The reaction was then started with the addition of H3K18-Ac peptide, tRNA, NAD^+ and DTT, performed for 2 h at 37°C and stopped by adding 50 µl of $HClO_4$ (15% in water). Samples were transferred to 96-well ELISA plates (Thermo Fisher Scientific) and 5 µl of the mixture was injected into the reverse phase ultra-fast liquid chromatography (RP-UFLC) system (Prominence Shimadzu UFLC system interfaced with LabSolutions software) for detection and quantification of the fluorescent H3K18 and H3K18-Ac peptides as previously described (Duval et al., 2015).

UV–visible absorption spectra

In order to evaluate the reactivity of NAC with quinones, a UV–visible absorbance test was performed based on the spectral properties of quinones (Satheeshkumar et al., 2014; Acharya et al., 2009; Dananjaya et al., 2012). Plumbagin, menadione, DMNQ or lawsone (150 µM) were mixed with or without 1.5 mM NAC, and incubated for 5 min at room temperature in 50 mM Tris-HCl, pH 8, 50 mM NaCl. The UV–visible absorbance spectrum was followed between 220 and 700 nm using a quartz tray on a spectrophotometer (UV-1650PC, Shimadzu, France).

GFP–Sirtuin 7 immunoprecipitation

GFP–Sirtuin 7 immunoprecipitation was performed on HeLa cells stably expressing GFP–Sirtuin 7 and on untreated HeLa cells as an immunoprecipitation control using the GFP-Trap Magnetic Agarose kit (ChromoTek) according to the manufacturer's instructions. About 20 million cells were harvested and then lysed with 400 µl of RIPA buffer (10 mM Tris-HCl, pH 7.5, 150 mM NaCl, 0.5 mM EDTA, 0.1% SDS, 1% Triton X-100, 1% deoxycholate) supplemented with 10 mM ascorbic acid, 5 mM $MgCl_2$, 0.1unit/µl DNase I (Roche) and protease inhibitors on ice for 30 min. The suspensions were extensively pipetted every 10 min and clarified by centrifugation (15,000 ***g***) for 20 min at 4°C. After taking an aliquot for Pierce BCA protein assay (Thermo Fisher Scientific), 1% 2-mercaptoethanol was added to inhibit further oxidation. After the protein assay was performed according to the manufacturer's instructions, protein samples (4 mg in 400 µl RIPA buffer supplemented with 1% 2-mercaptoethanol) were made up to 1 ml with dilution/wash buffer (10 mM Tris-HCl, pH 7.5, 150 mM NaCl, 0.5 mM EDTA) supplemented with 1% 2-mercaptoethanol and protease inhibitors, and then incubated at 4°C overnight with 20 µl equilibrated magnetic agarose beads. The beads were then pelleted by centrifugation (400 ***g***) for 3 min at 4°C and washed three

times with the dilution/wash buffer supplemented with 1% 2-mercaptoethanol and protease inhibitors. The supernatants were saved and adjusted to 6% SDS. After washing, beads were resuspended in 20 µl of RIPA buffer adjusted to 6% SDS, boiled for 10 min at 95°C and separated with a magnet. The eluates and supernatants were then analyzed with the OxyBlot kit (Merck) and anti-Sirtuin 7 antibody.

OxyBlot procedure

Protein extracts were prepared from cells lysed in PBS pH 7.4, 500 mM NaCl, 6% SDS, 2% 2-mercaptoethanol and protease inhibitors, and the eluates and supernatants prepared as reported above were used for analyses with the OxyBlot kit. Protein samples (10 µl) were first derivatized by adding the same volume of 2,4-dinitrophenylhydrazine (DNPH) solution and incubating the mixture at room temperature for 15 min. The mixture was then neutralized by adding the neutralization solution (7.5 µl). After adding 2-mercaptoethanol (5% vol/vol), the DNP-derivatized protein samples were separated by SDS-PAGE and analyzed by immunoblotting using a rabbit anti-DNP antibody, followed by a horseradish peroxidase-conjugated goat ant-rabbit antibody. The immunoreactivity is then detected by chemiluminescence and quantified with ImageJ software (NIH).

Northern blot analysis

For northern blot analyses, total RNA was extracted from cells using NucleoSpin RNA (Macherey-Nagel), separated (4 µg) in 0.8% agarose formaldehyde gels and transferred to positively charged membranes (Roche). Hybridization was carried out using DIG Easy Hyb buffer (Roche) at 50°C. After washing, the probe was revealed using the DIGWash and Block Buffer Set (Roche) and the alkaline-phosphatase-conjugated anti-digoxigenin antibodies. Alkaline phosphatase activity was detected using the chemiluminescent substrate CDP-Star (Roche) and quantified with ImageJ software.

Statistical analysis

Statistical analyses were performed using one-way analysis of variance (ANOVA) followed by Dunnet's post hoc test, Kruskal–Wallis followed by Dunn's post hoc test or Mann–Whitney rank test if only two groups were compared, with Prism 5.03 software (GraphPad Software).

Acknowledgements

The authors thank the imaging platform of the Unité de Biologie Fonctionnelle et Adaptative, Linh Chi Bui and the platform Bioprofiler of the facility 'Métabolisme' of the Unité de Biologie Fonctionnelle et Adaptative.

Competing interests

The authors declare no competing or financial interests.

Author contributions

Conceptualization: V.S., J.B., P.R.; Methodology: V.S., J.B., P.R.; Software: O.B.; Validation: V.S., J.B., P.R.; Formal analysis: V.S., J.B., P.R.; Investigation: V.S., J.B., P.R.; Resources: V.S., P.R.; Data curation: P.R.; Writing - original draft: V.S., P.R.; Writing - review & editing: O.B., P.R.; Visualization: V.S., P.R.; Supervision: P.R.

Funding

This study was supported by grants from the Centre National de la Recherche Scientifique and the Université Paris Cité. J.B. was supported by a PhD fellowship from Cancéropôle Île-de-France. O.B. was employed as a postdoctoral researcher on the ANR-17-CE09-0017 project funded by the Agence Nationale de la Recherche (AlveolusMimics).

References

Acharya, B. R., Choudhury, D., Das, A. and Chakrabarti, G. (2009). Vitamin K3 disrupts the microtubule networks by binding to tubulin: a novel mechanism of its antiproliferative activity. *Biochemistry* **48**, 6963-6974. doi:10.1021/bi900152k

Barber, M. F., Michishita-Kioi, E., Xi, Y., Tasselli, L., Kioi, M., Moqtaderi, Z., Tennen, R. I., Paredes, S., Young, N. L., Chen, K. et al. (2012). SIRT7 links H3K18 deacetylation to maintenance of oncogenic transformation. *Nature* **487**, 114-118. doi:10.1038/nature11043

Blander, G. and Guarente, L. (2004). The Sir2 family of protein deacetylases. *Annu. Rev. Biochem.* **73**, 417-435. doi:10.1146/annurev.biochem.73.011303.073651

Boulon, S., Westman, B. J., Hutten, S., Boisvert, F. M. and Lamond, A. I. (2010). The nucleolus under stress. *Mol. Cell* **40**, 216-227. doi:10.1016/j.molcel.2010.09.024

Bywater, M. J., Poortinga, G., Sanij, E., Hein, N., Peck, A., Cullinane, C., Wall, M., Cluse, L., Drygin, D., Anderes, K. et al. (2012). Inhibition of RNA polymerase i as a therapeutic strategy to promote cancer-specific activation of p53. *Cancer Cell* **22**, 51-65. doi:10.1016/j.ccr.2012.05.019

Cao, Y.-Y., Yu, J., Liu, T.-T., Yang, K.-X., Yang, L.-Y., Chen, Q., Shi, F., Hao, J.-J., Cai, Y., Wang, M.-R. et al. (2018). Plumbagin inhibits the proliferation and survival of esophageal cancer cells by blocking STAT3-PLK1-AKT signaling article. *Cell Death Dis.* **9**, 17. doi:10.1038/s41419-017-0068-6

Carr, B. I., Wang, Z. and Kar, S. (2002). K vitamins, PTP antagonism, and cell growth arrest. *J. Cell. Physiol.* **193**, 263-274. doi:10.1002/jcp.10171

Checker, R., Sharma, D., Sandur, S. K., Khanam, S. and Poduval, T. B. (2009). Anti-inflammatory effects of plumbagin are mediated by inhibition of NF-kappaB activation in lymphocytes. *Int. Immunopharmacol.* **9**, 949-958. doi:10.1016/j.intimp.2009.03.022

Chen, S., Blank, M. F., Iyer, A., Huang, B., Wang, L., Grummt, I. and Voit, R. (2016). SIRT7-dependent deacetylation of the U3-55k protein controls pre-rRNA processing. *Nat. Commun.* **7**, 10734. doi:10.1038/ncomms10734

Chen, K. L., Li, L., Yang, F. X., Li, C. M., Wang, Y. R. and Wang, G. L. (2018). SIRT7 depletion inhibits cell proliferation, migration, and increases drug sensitivity by activating p38MAPK in breast cancer cells. *J. Cell. Physiol.* **233**, 6767-6778. doi:10.1002/jcp.26398

Dananjaya, S. H. S., Edussuriya, M. and Dissanayake, A. S. (2012). Inhibition action of lawsone on the corrosion of mild steel in acidic media. *Online J. Sci. Technol.* **2**, 32-36.

Duval, R., Fritsch, L., Bui, L.-C., Berthelet, J., Guidez, F., Mathieu, C., Dupret, J.-M., Chomienne, C., Ait-Si-Ali, S. and Rodrigues-Lima, F. (2015). An acetyltransferase assay for CREB-binding protein based on reverse phase-ultra-fast liquid chromatography of fluorescent histone H3 peptides. *Anal. Biochem.* **486**, 35-37. doi:10.1016/j.ab.2015.06.024

Duval, R., Bui, L. C., Mathieu, C., Nian, Q., Berthelet, J., Xu, X., Haddad, I., Vinh, J., Dupret, J.-M., Busi, F. et al. (2019). Benzoquinone, a leukemogenic metabolite of benzene, catalytically inhibits the protein tyrosine phosphatase PTPN2 and alters STAT1 signaling. *J. Biol. Chem.* **294**, 12483-12494. doi:10.1074/jbc.RA119.008666

Ford, E., Voit, R., Liszt, G., Magin, C., Grummt, I. and Guarente, L. (2006). Mammalian Sir2 homolog SIRT7 is an activator of RNA polymerase I transcription. *Genes Dev.* **20**, 1075-1080. doi:10.1101/gad.1399706

Grob, A., Roussel, P., Wright, J. E., McStay, B., Hernandez-Verdun, D. and Sirri, V. (2009). Involvement of SIRT7 in resumption of rDNA transcription at the exit from mitosis. *J. Cell Sci.* **122**, 489-498. doi:10.1242/jcs.042382

Iwamoto, N., Sumi, D., Ishii, T., Uchida, K., Cho, A. K., Froines, J. R. and Kumagai, Y. (2007). Chemical knockdown of protein-tyrosine phosphatase 1B by 1,2-naphthoquinone through covalent modification causes persistent transactivation of epidermal growth factor receptor. *J. Biol. Chem.* **282**, 33396-33404. doi:10.1074/jbc.M705224200

Jing, L., Lin, S., Lu, F. R., You, Q., Rui, C., Jia, L., Yan, L., Zhan, H. Z. and He, Y. Q. (2012). Plumbagin inhibits cell growth and potentiates apoptosis in human gastric cancer cells in vitro through the NF-B signaling pathway. *Acta Pharmacol. Sin.* **33**, 242-249. doi:10.1038/aps.2011.152

Joo, M. K., Park, J. J., Kim, S. H., Yoo, H. S., Lee, B. J., Chun, H. J., Lee, S. W. and Bak, Y. T. (2015). Antitumorigenic effect of plumbagin by induction of SH2-containing protein tyrosine phosphatase 1 in human gastric cancer cells. *Int. J. Oncol.* **46**, 2380-2388. doi:10.3892/ijo.2015.2935

Kar, S., Lefterov, I. M., Wang, M., Lazo, J. S., Scott, C. N., Wilcox, C. S. and Carr, B. I. (2003). Binding and inhibition of Cdc25 phosphatases by vitamin K analogues. *Biochemistry* **42**, 10490-10497. doi:10.1021/bi027418p

Kim, J. H., Kim, D., Cho, S. J., Jung, K. Y., Kim, J. H., Lee, J. M., Jung, H. J. and Kim, K. R. (2019). Identification of a novel SIRT7 inhibitor as anticancer drug candidate. *Biochem. Biophys. Res. Commun.* **508**, 451-457. doi:10.1016/j.bbrc.2018.11.120

Klaus, V., Hartmann, T., Gambini, J., Graf, P., Stahl, W., Hartwig, A. and Klotz, L. O. (2010). 1,4-Naphthoquinones as inducers of oxidative damage and stress signaling in HaCaT human keratinocytes. *Arch. Biochem. Biophys.* **496**, 93-100. doi:10.1016/j.abb.2010.02.002

Klotz, L.-O., Patak, P., Ale-Agha, N., Buchczyk, D. P., Abdelmohsen, K., Gerber, P. A., Von Montfort, C. and Sies, H. (2002). 2-Methyl-1,4-naphthoquinone, vitamin K3, decreases gap-junctional intercellular communication via activation of the epidermal growth factor receptor/extracellular signal-regulated kinase cascade. *Cancer Res.* **62**, 4922-4928.

Klotz, L.-O., Hou, X. and Jacob, C. (2014). 1,4-naphthoquinones: from oxidative damage to cellular and inter-cellular signaling. *Molecules* **19**, 14902-14918. doi:10.3390/molecules190914902

Kumagai, Y., Shinkai, Y., Miura, T. and Cho, A. K. (2012). The chemical biology of naphthoquinones and its environmental implications. *Annu. Rev. Pharmacol. Toxicol.* **52**, 221-247. doi:10.1146/annurev-pharmtox-010611-134517

Laemmli, U. K. (1970). Cleavage of structural proteins during the assembly of the head of bacteriophage T4. *Nature* **227**, 680-685. doi:10.1038/227680a0

Langhendries, J. -L., Nicolas, E., Doumont, G., Goldman, S. and Lafontaine, D. L. (2016). The human box C/D snoRNAs U3 and U8 are required for pre-rRNA processing and tumorigenesis. *Oncotarget* **7**, 59519-59534. doi:10.18632/oncotarget.11148

Michishita, E., Park, J. Y., Burneskis, J. M., Carl Barrett, J. and Horikawa, I. (2005). Evolutionarily conserved and nonconserved cellular localizations and functions of human SIRT proteins. *Mol. Biol. Cell* **16**, 4623-4635. doi:10.1091/mbc.e05-01-0033

Mitra, N. and Dey, S. (2020). Biochemical characterization of mono ADP ribosyl transferase activity of human sirtuin SIRT7 and its regulation. *Arch. Biochem. Biophys.* **680**, 108226. doi:10.1016/j.abb.2019.108226

Nian, Q., Berthelet, J., Zhang, W., Bui, L.-C., Liu, R., Xu, X., Duval, R., Ganesan, S., Leger, T., Chomienne, C. et al. (2019). T-cell protein tyrosine phosphatase is irreversibly inhibited by etoposide-quinone, a reactive metabolite of the chemotherapy drug etoposide. *Mol. Pharmacol.* **96**, 297-306. doi:10.1124/mol.119.116319

Popov, A., Smirnov, E., Kováčik, L., Raška, O., Hagen, G., Stixová, L. and Raška, I. (2013). Duration of the first steps of the human rRNA processing. *Nucleus* **4**, 134-141. doi:10.4161/nucl.23985

Qiu, H.-Y., Wang, P.-F., Lin, H.-Y., Tang, C.-Y., Zhu, H.-L. and Yang, Y.-H. (2018). Naphthoquinones: a continuing source for discovery of therapeutic antineoplastic agents. *Chem. Biol. Drug Des.* **91**, 681-690. doi:10.1111/cbdd.13141

Rajendran, R., Garva, R., Krstic-Demonacos, M. and Demonacos, C. (2011). Sirtuins: molecular traffic lights in the crossroad of oxidative stress, chromatin remodeling, and transcription. *J. Biomed. Biotechnol.* **2011**, 368276. doi:10.1155/2011/368276

Rogakou, E. P., Pilch, D. R., Orr, A. H., Ivanova, V. S. and Bonner, W. M. (1998). DNA double-stranded breaks induce histone H2AX phosphorylation on serine 139. *J. Biol. Chem.* **273**, 5858-5868. doi:10.1074/jbc.273.10.5858

Sandur, S. K., Pandey, M. K., Sung, B. and Aggarwal, B. B. (2010). 5-Hydroxy-2-methyl-1,4-naphthoquinone, a vitamin K3 analogue, suppresses STAT3 activation pathway through induction of protein tyrosine phosphatase, SHP-1: Potential role in chemosensitization. *Mol. Cancer Res.* **8**, 107-118. doi:10.1158/1541-7786.MCR-09-0257

Satheeshkumar, K., Jose, B., Dhanya, B. P. and Krishnan, P. N. (2014). Prospects of Plumbago rosea L. hairy root culture in traditional preparations: A phytochemical comparison with tuberous roots. *Plant Root* **8**, 13-23. doi:10.3117/plantroot.8.13

Singh, C. K., Chhabra, G., Ndiaye, M. A., Garcia-Peterson, L. M., MacK, N. J. and Ahmad, N. (2018). The role of sirtuins in antioxidant and redox signaling. *Antioxidants Redox Signal.* **28**, 643-661. doi:10.1089/ars.2017.7290

Sirri, V., Hernandez-Verdun, D. and Roussel, P. (2002). Cyclin-dependent kinases govern formation and maintenance of the nucleolus. *J. Cell Biol.* **156**, 969-981. doi:10.1083/jcb.200201024

Sirri, V., Jourdan, N., Hernandez-Verdun, D. and Roussel, P. (2016). Sharing of mitotic pre-ribosomal particles between daughter cells. *J. Cell Sci.* **129**, 1592-1604. doi:10.1242/jcs.180521

Sirri, V., Grob, A., Berthelet, J., Jourdan, N. and Roussel, P. (2019). Sirtuin 7 promotes 45S pre-rRNA cleavage at site 2 and determines the processing pathway. *J. Cell Sci.* **132**, jcs.228601. doi:10.1242/jcs.228601

Stadtman, E. R. (1993). Oxidation of free amino acids and amino acid residues in proteins by radiolysis and by metal-catalyzed reactions. *Annu. Rev. Biochem.* **62**, 797-821. doi:10.1146/annurev.bi.62.070193.004053

Sun, L. and Fang, J. (2016). Macromolecular crowding effect is critical for maintaining SIRT1's nuclear localization in cancer cells. *Cell Cycle* **15**, 2647-2655. doi:10.1080/15384101.2016.1211214

Tamura, K., Southwick, E. C., Kerns, J., Rosi, K., Carr, B. I., Wilcox, C. and Lazo, J. S. (2000). Cdc25 inhibition and cell cycle arrest by a synthetic thioalkyl vitamin K analogue. *Cancer Res.* **60**, 1317-1325.

Tang, M., Lu, X., Zhang, C., Du, C., Cao, L., Hou, T., Li, Z., Tu, B., Cao, Z., Li, Y. et al. (2017). Downregulation of SIRT7 by 5-fluorouracil induces radiosensitivity in human colorectal cancer. *Theranostics* **7**, 1346-1359. doi:10.7150/thno.18804

Tang, M., Li, Z., Zhang, C., Lu, X., Tu, B., Cao, Z., Li, Y., Chen, Y., Jiang, L., Wang, H. et al. (2019). SIRT7-mediated ATM deacetylation is essential for its deactivation and DNA damage repair. *Sci. Adv.* **5**, eaav1118. doi:10.1126/sciadv.aav1118

Tripathi, S. K., Panda, M. and Biswal, B. K. (2019). Emerging role of plumbagin: cytotoxic potential and pharmaceutical relevance towards cancer therapy. *Food Chem. Toxicol.* **125**, 566-582. doi:10.1016/j.fct.2019.01.018

Vasudevarao, M. D., Mizar, P., Kumari, S., Mandal, S., Siddhanta, S., Swamy, M. M., Kaypee, S., Kodihalli, R. C., Banerjee, A., Naryana, C. et al. (2014). Naphthoquinone-mediated inhibition of lysine acetyltransferase KAT3B/p300, basis for non-toxic inhibitor synthesis. *J. Biol. Chem.* **289**, 7702-7717. doi:10.1074/jbc.M113.486522

Vazquez, B. N., Thackray, J. K., Simonet, N. G., Kane–Goldsmith, N., Martinez–Redondo, P., Nguyen, T., Bunting, S., Vaquero, A., Tischfield, J. A. and Serrano, L. (2016). SIRT 7 promotes genome integrity and modulates non–homologous end joining DNA repair. *EMBO J.* **35**, 1488-1503. doi:10.15252/embj.201593499

Wang, X. X., Wang, X. L., Tong, M.-m., Gan, L., Chen, H., Wu, S.-s., Chen, J. X., Li, R. L., Wu, Y., Zhang, H.-y. et al. (2016). SIRT6 protects cardiomyocytes against ischemia/reperfusion injury by augmenting FoxO3α-dependent antioxidant defense mechanisms. *Basic Res. Cardiol.* **111**, 1-19. doi:10.1007/s00395-016-0531-z

Wellington, K. W. (2015). Understanding cancer and the anticancer activities of naphthoquinones-a review. *RSC Adv.* **5**, 20309-20338. doi:10.1039/C4RA13547D

Wu, F. Y. H. and Sun, T. P. (1999). Vitamin K3 induces cell cycle arrest and cell death by inhibiting Cdc25 phosphatase. *Eur. J. Cancer* **35**, 1388-1393. doi:10.1016/S0959-8049(99)00156-2

Yang, K., Wang, M., Zhao, Y., Sun, X., Yang, Y., Li, X., Zhou, A., Chu, H., Zhou, H., Xu, J. et al. (2016). A redox mechanism underlying nucleolar stress sensing by nucleophosmin. *Nat. Commun.* **7**, 13599. doi:10.1038/ncomms13599

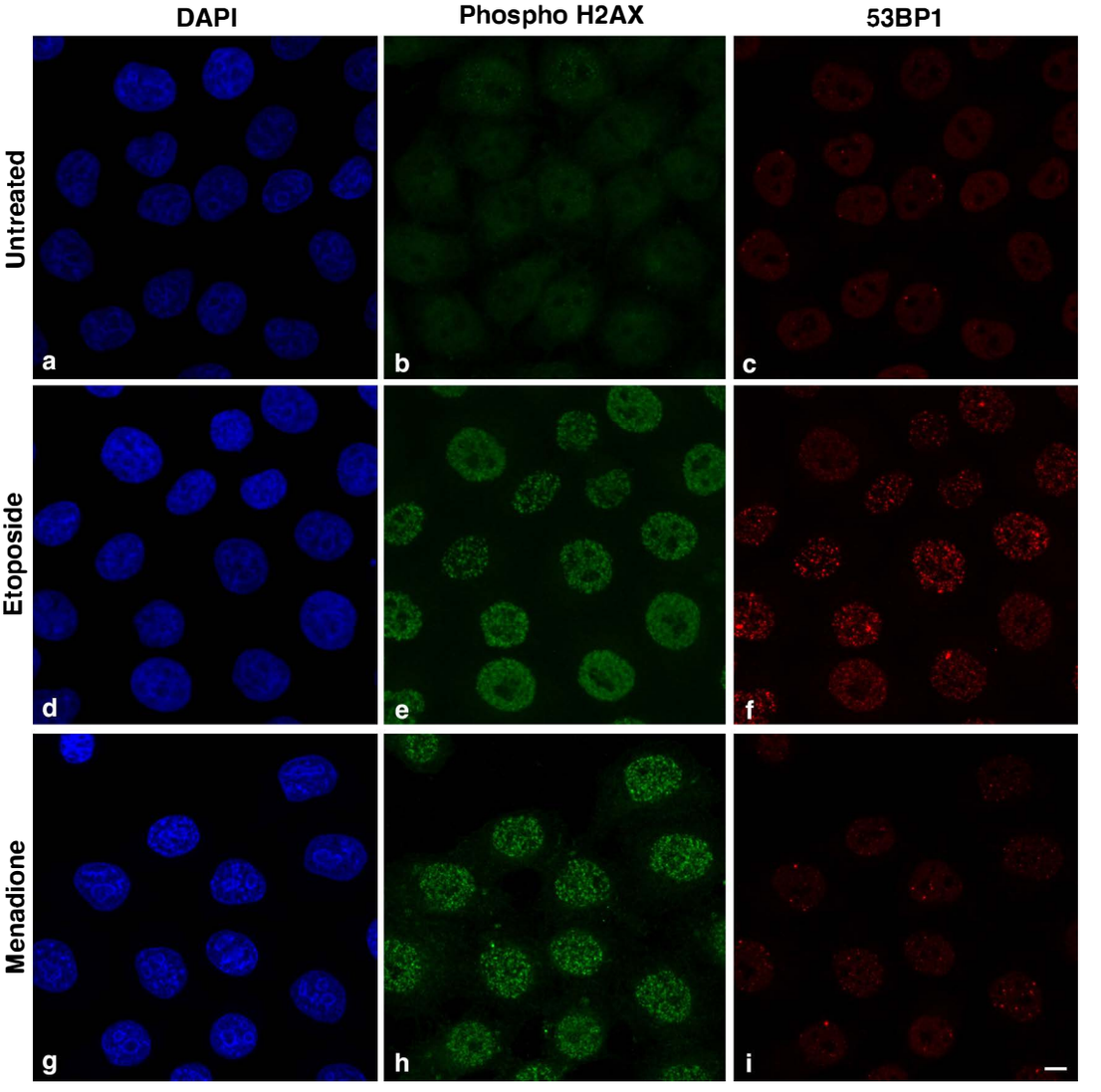

Fig. S1. Menadione impairs DNA repair *in vivo*. (A) The recruitment of 53BP1 to DNA double-strand breaks was analysed in HeLa cells treated with 20 µM etoposide (d-f) or 40 µM menadione (g-i) for 30 min, or not treated (a-c). Immunofluorescence labelling was performed using anti-phospho H2AX (b, e and h) and anti-53BP1 (c, f and i) antibodies. Z-maximum projections are shown. Scale bar: 10 µm.

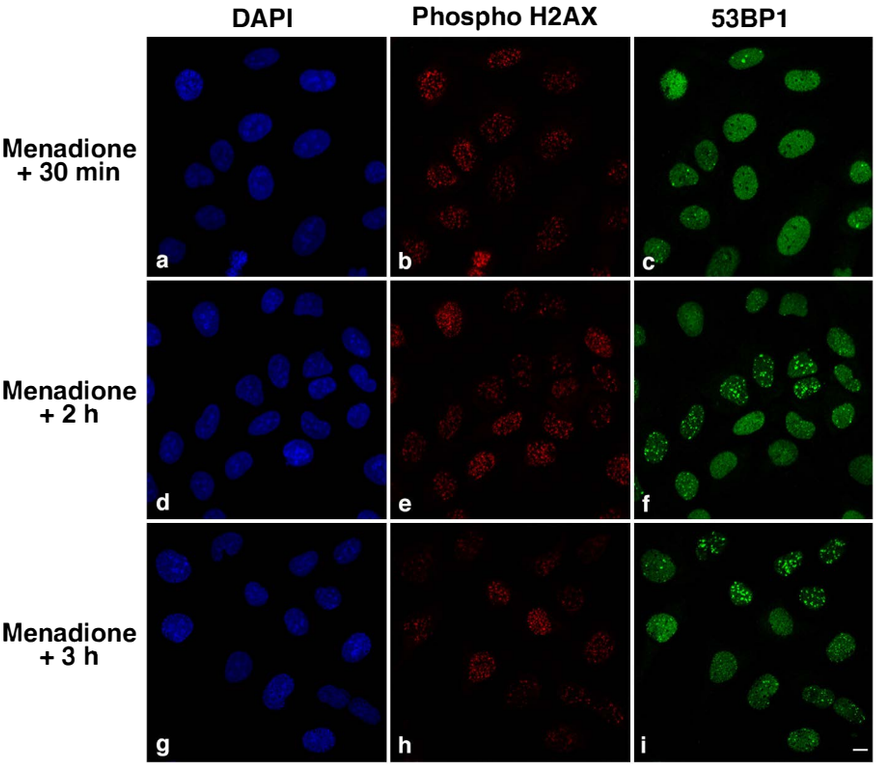

Fig. S2. Menadione-induced inhibition of 53BP1 foci formation can be reversed. The recruitment of 53BP1 to DNA double-strand breaks was analysed in U2OS cells treated with 60 µM menadione for 30 min, washed and cultured for additional 30 min, 2 or 3 h. Immunofluorescence labelling was performed using anti-phospho H2AX (b, e and h) and anti-53BP1 (c, f and i) antibodies. Z-maximum projections are shown. Scale bar: 10 µm.

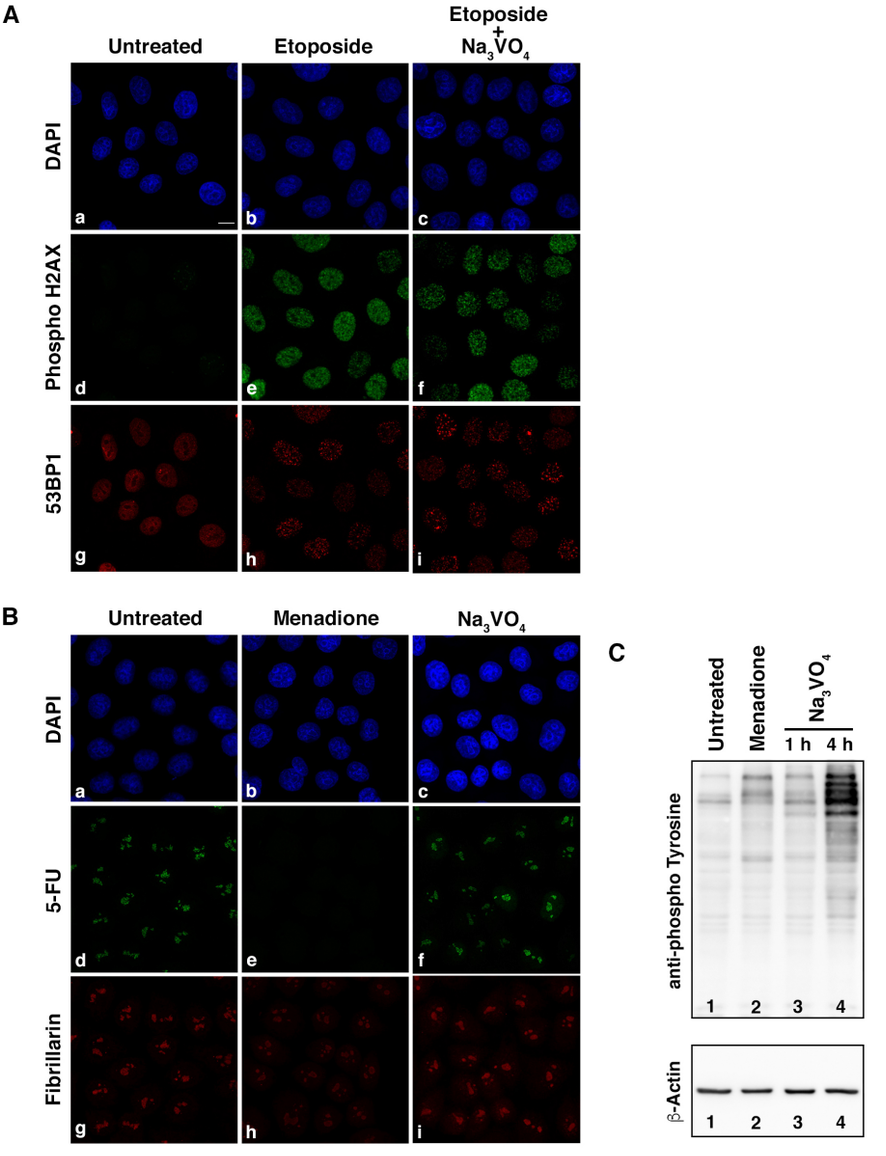

Fig. S3. Etoposide-induced 53BP1 foci formation and rDNA transcription are not influenced by Na_3VO_4 treatment. (A) The recruitment of 53BP1 to DNA double-strand breaks was analysed in HeLa cells treated or not treated with 1 mM Na_3VO_4 for 4 h and cultured for additional 30 min with or without 20 µM etoposide. Immunofluorescence labelling was performed using anti-phospho H2AX (d-f) and anti-53BP1 (g-i) antibodies. (B) HeLa cells were treated or not treated with either 40 µM menadione for 1 h or 1 mM Na_3VO_4 for 4 h, and cultured in medium containing 5-FU for the last 15 min of culture before being processed to reveal 5-FU incorporation (d-f) and to observe fibrillarin (g-i). Z-maximum projections are shown. Scale bar: 10 µm. (C) Immunoblot analysis of extracts prepared from HeLa cells untreated (1) or treated with either 40 µM menadione for 1 h (2) or 1 mM Na_3VO_4 for 1 h (3) or 4 h (4) using the anti-phospho-Tyrosine antibody. After membrane stripping, analysis was carried out using the anti-β-Actin antibody.

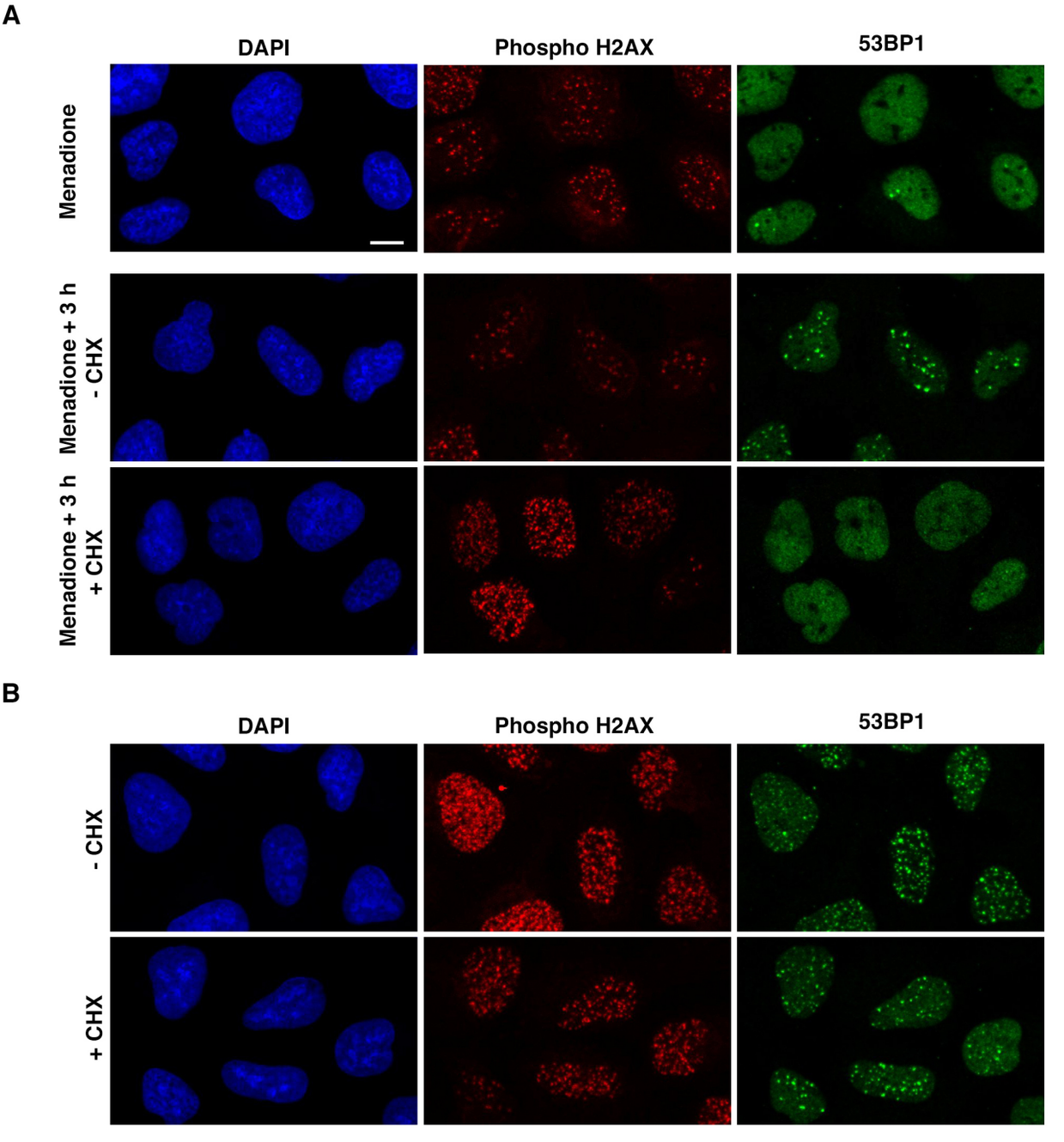

Fig. S4. Menadione-induced inhibition of 53BP1 foci formation is no longer reversed in the presence of CHX. (A) The recruitment of 53BP1 to DNA double-strand breaks was analysed in U2OS cells treated with 60 µM menadione for 30 min, washed and cultured for additional 3 h in the presence or in the absence of CHX (50 µg/ml). (B) The recruitment of 53BP1 to DNA double-strand breaks was analysed in U2OS cells cultured for 3 h in the presence or in the absence of CHX (50 µg/ml). Etoposide (20 µM) was added for the last 30 min to induce DNA double-strand breaks. Immunofluorescence labelling was performed using anti-phospho H2AX and anti-53BP1 antibodies. Z-maximum projections are shown. Scale bar: 10 µm.

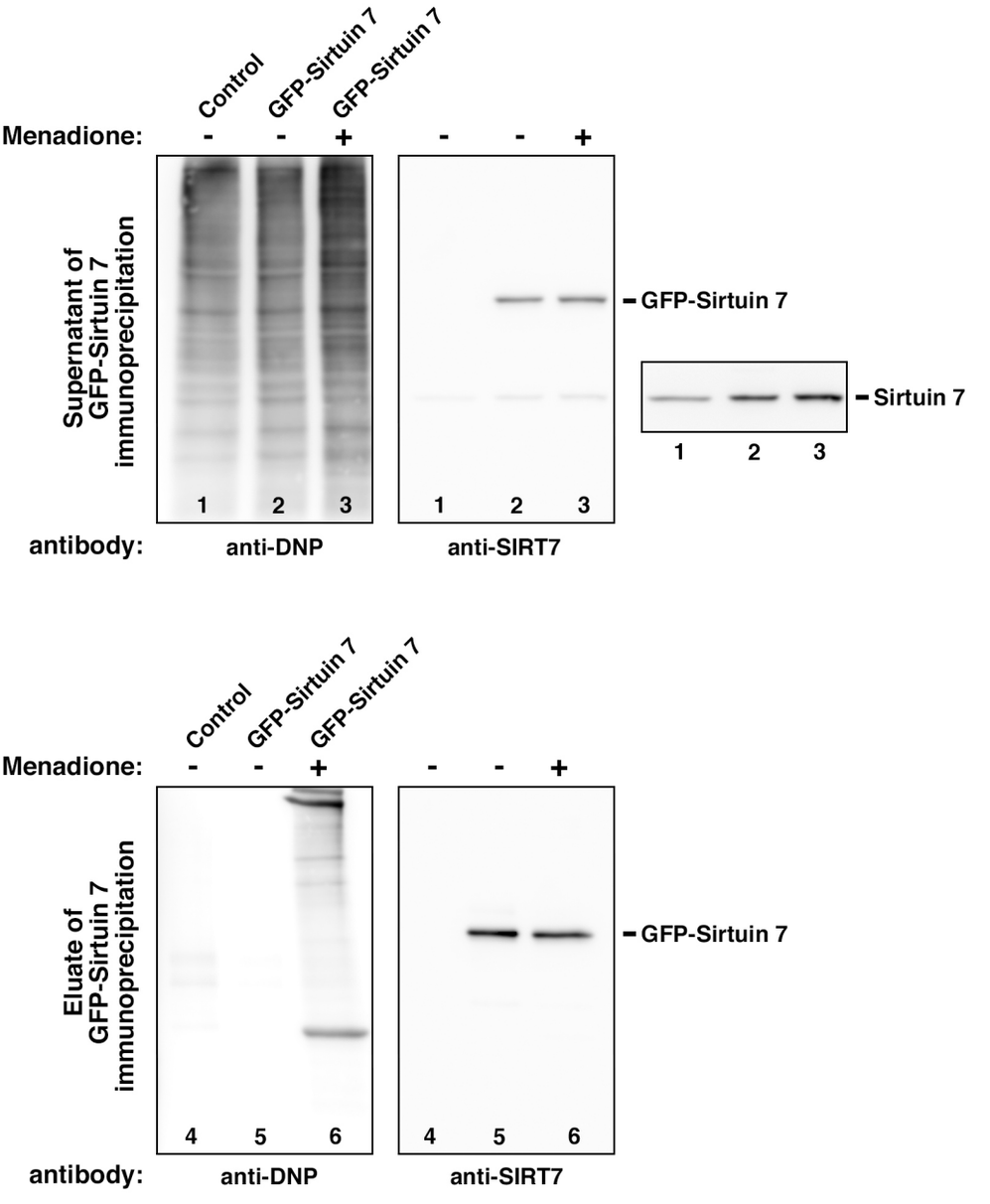

Fig. S5. Inhibition of Sirtuin 7 is not linked to oxidative modifications. HeLa cells expressing Sirtuin 7-GFP were treated or not with 40 µM menadione for 2 h, lysed and processed for GFP-Sirtuin 7 immunoprecitation. Potential oxidative modifications of GFP-Sirtuin 7 were analysed on supernatants and eluates using the OxyBlot Protein Oxidation Detection Kit. DNP-derivatized protein samples were separated by SDS-PAGE and revealed by immunoblotting using first anti-DNP antibody and then anti-Sirtuin 7 antibody. The cropped part of the signal corresponding to endogenous Sirtuin 7 present in the supernatants is presented on the right after applying a global intensity adjustment.